

# Analysis of Orbital Decay Time for the Classical Hydrogen Atom Interacting with Circularly Polarized Electromagnetic Radiation

Daniel C. Cole and Yi Zou

Dept. of Manufacturing Engineering, 15 St. Mary's Street,  
Boston University, Brookline, MA 02446

## Abstract

Here we show that a wide range of states of phases and amplitudes exist for a circularly polarized (CP) plane wave to act on a classical hydrogen model to achieve infinite times of stability (i.e., no orbital decay due to radiation reaction effects). An analytic solution is first deduced to show this effect for circular orbits in the nonrelativistic approximation. We then use this analytic result to help provide insight into detailed simulation investigations of deviations from these idealistic conditions. By changing the phase of the CP wave, the time  $t_d$  when orbital decay sets in can be made to vary enormously. The patterns of this behavior are examined here and analyzed in physical terms for the underlying but rather unintuitive reasons for these nonlinear effects. We speculate that most of these effects can be generalized to analogous elliptical orbital conditions with a specific infinite set of CP waves present. The article ends by briefly considering multiple CP plane waves acting on the classical hydrogen atom in an initial circular orbital state, resulting in “jump- and diffusion-like” orbital motions for this highly nonlinear system. These simple examples reveal the possibility of very rich and complex patterns that occur when a wide spectrum of radiation acts on this classical hydrogen system.

## I. INTRODUCTION

The hydrogen atom has received renewed attention in the past decade or so, due to studies involved with Rydberg analysis, chaos, and scarring [1], [2], [3], [4]. Classical and semiclassical analysis have been found in the past to offer helpful insight and predictability on the behavior of Rydberg-like atoms. However, in these previous interesting works involving classical and semiclassical analyses of ionization behavior and chaotic and scarred orbits of Rydberg systems (see, for example, Refs. [5], [2], [6], [3], [7], [8], and cited references therein), the radiation reaction term in the Lorentz-Dirac equation [9] describing the behavior of classical charged point particles is rarely, if at all, considered. Although physicists certainly agree that this term is necessary in a consistent classical electrodynamic treatment of classical charged particles [9], [10], [11], [12], still, this is the term that persuaded physicists in the early 1900s that a completely classical treatment of the atom was not a viable explanation for atomic behavior, as it would necessarily result in a collapse of the electron's orbit in a time of about  $1.3 \times 10^{-11}$  sec. This observation, and other apparently nonclassical effects (blackbody radiation, photoelectric effect, etc.), spurred the development of Bohr's atomic model, followed by the more complete work by Heisenberg, Schrödinger, Dirac, and others of quantum mechanics.

Nevertheless, our recent work [13], [14], [15] has revealed a number of interesting situations as a result of the very nonlinear behavior of the Coulombic binding potential, as well as the small but steady action of the radiation reaction damping force, and the presence of applied electromagnetic radiation acting on the classical atom. Our intention is to continue this development, building upon previous work to include the effects of multiple plane waves. We expect at the very least to continue to uncover interesting and surprising results of the nonlinear behavior of this classical system. However, we also expect that the results may prove helpful in revealing better why the classical analysis can in some cases provide excellent insight into the behavior of Rydberg atomic systems. For example, the literature is full of such observations, such as in the extensive report of Ref. [2], p. 291: "Where the quantitative agreement between experimental data and classical calculations is good for threshold field amplitudes for the onset of 'ionization', the classical theory gives keen insight into the semiclassical dynamics. Conversely, where the quantitative agreement breaks down is a signature for the importance of quantal effects. Often this occurs where the nonclassical

behavior is, nevertheless, still anchored in subtle ways to the classical dynamics in and near nonlinear resonances.” Pushing on such understanding should prove to be helpful in modeling, as simply as possible, the surprisingly complex behavior that has been reported for Rydberg-like systems. We are hopeful to be able to use such models in technology application situations.

Finally, at the most, we are hopeful to uncover more of when, why, and possibly why not, the theory of stochastic electrodynamics (SED) holds for the simple classical hydrogen atom. As reported in much more detail elsewhere [15], [16], [17], [18], SED is an entirely classical theory of nature that considers the interaction of classical charged particles with electromagnetic fields, using Maxwell’s classical electromagnetic equations, but while also considering that an equilibrium situation for particles and fields at temperature  $T = 0$  necessarily requires the presence of classical electromagnetic zero-point (ZP) radiation. This idea has revealed a number of surprisingly quantum mechanical-like properties to be predicted from this entirely classical theory. However, when attacking realistic atomic systems in nature, rather than simple approximate systems like the simple harmonic oscillator, then severe difficulties have been reported in the past [17],[18]. We have been suspicious that some of these difficulties may simply be due to the inherent difficulty of analyzing the subtle nonlinear effects of a Coulombic binding potential [19],[20]; the present study, along with other work to be presented in the near future, is intended to help address some of these points.

Indeed, our work in Ref. [21] shows that a detailed simulation of the effects of classical electromagnetic radiation acting on a classical electron in a classical hydrogen potential, results in a stochastic-like motion that yields a probability distribution over time that appears extremely close to the ground state probability distribution for hydrogen. Clearly there are tantalizing physical aspects yet to be understood here of the ramifications of this work. These particular simulations are extremely computationally intensive. However, for large orbits, as would typically occur in a Rydberg atom, the computations would become enormously smaller, thereby providing an efficient computational tool for addressing Rydberg atom behavior. Thus, in summary, we believe this research direction should provide an excellent technology related simulation tool for studying much of Rydberg atom dynamics, while also providing the means for understanding much deeper ramifications of SED and its possible basis for much of quantum mechanics.

Except for a preliminary result to be considered in the concluding section of this article involving many plane waves, the present article considers a single classical circularly polarized (CP) plane wave interacting with the classical hydrogen atom. This atomic system will be treated here as consisting of a particle with charge  $-e$  and rest mass  $m$ , orbiting an infinitely massive and oppositely charged nucleus. In Ref. [15] we carried out a perturbation analysis, showing in more detail why some of the nonlinear behaviors occur as first discussed in Ref. [13]. In particular, for the classical electron moving in a near circular orbit, with an applied CP plane wave normally directed at the plane of the orbit, then quasi-stability of the orbit can be achieved provided the amplitude of the electric field of plane wave exceeds a particular critical value. The result is a constant spiralling in and out motion of the electron, with the spirals growing larger and larger in amplitude, until finally a critical point is reached and then decay of the orbit occurs. As shown in Ref. [14], this same behavior also occurs for more general, but more complicated, elliptical orbits, where now an infinite set of plane waves are required to achieve the same effect, where the plane waves are harmonics of the period of the orbit.

In Sec. II of the present article, we begin by providing more general conditions than considered in Ref. [13] for achieving perfect stability for the interaction of a single CP wave with the classical hydrogen atom. This example will provide a clearer physical insight into why the effect of the phase of the CP plane wave, in relation to the motion of the orbiting electron, is so extremely important in changing the time to decay,  $t_d$ , of the classical electron's orbit. Section III then turns to a detailed simulation analysis of a wide range of conditions influencing  $t_d$ . Many of these results seem physically very unintuitive. Section IV then turns to explain and analyze some of these subtleties, by making use of some of the perturbation work in Ref. [15].

Finally, Sec. V ends with a few concluding remarks on where we anticipate this work is headed. Future articles are intended to report on work already finished or in various stages of completion, including a full relativistic examination, and the situation that is of great interest to us, namely, when a radiation spectrum is present that may possibly result in a thermodynamic equilibrium state with the classical atom. In anticipation of this work, in Sec. V we briefly examine the interesting question of what happens when multiplane waves act on the orbiting electron. As should be evident from Refs. [13], [14], and [15], this simple classical hydrogen problem presents a rich range of interesting nonlinear phenomena with

just the simple consideration of a single electromagnetic plane wave acting. However, with multiple plane waves, the range of possibilities grows considerably wider, as illustrated in Sec. V. As shown there, “jump-like” behaviors are fairly easy to create.

## II. ANALYSIS OF INFINITE STABILITY CASE

As discussed in Ref. [13], when a classical electron of mass  $m$ , charge  $-e$ , follows a circular orbit of radius  $a$  about an infinitely massive and oppositely charged point nucleus, and when a CP plane wave is directed along the normal to the plane of the orbit, then by choosing the frequency of the plane wave to be equal to the orbital frequency, or  $\omega_c \equiv \left(\frac{e^2}{ma^3}\right)^{1/2}$ , and by choosing the phase of the velocity of the electron and the electric field to be aligned with each other (i.e., make  $(-e)\mathbf{E}$  to be in the same direction as the velocity  $\dot{\mathbf{z}}$ ), then the amplitude  $A$  of the electric field of the plane wave can be chosen to perfectly balance the radiation reaction. The condition found was

$$A_c \equiv \frac{2e^3\omega_c}{3mc^3a^2} = (\omega_c\tau) \frac{e}{a^2} \quad . \quad (1)$$

where  $\tau \equiv \frac{2e^2}{3mc^3}$ .

However, we can generalize this very specific scenario and achieve similar conditions of perfect stability for the case when  $A > A_c$ . Figure 1 illustrates the basic idea. By having the component of the force  $(-e)\mathbf{E}$  from the plane wave in the  $x - y$  plane, of  $eA \cos(\alpha)$ , be equal and opposite to the radiation reaction, then the angular frequency of the orbiting particle can stay constant. Moreover, by allowing a slightly different angular frequency in the orbiting motion from what would occur if the particle was only under the influence of the Coulombic binding potential, so that now we allow  $\omega \neq \omega_c$ , then an orbit of constant radius  $a$  can be maintained.

Being more specific, we can write the nonrelativistic (NR) equations of motion in polar coordinates as:

$$m \left( \ddot{r} - r\dot{\theta}^2 \right) = -\frac{e^2}{r^2} + 2\tau e^2 \frac{\dot{r}}{r^3} + eA \sin(\theta - \omega t - \alpha) \quad , \quad (2)$$

and

$$m \left( r\ddot{\theta} + 2\dot{r}\dot{\theta} \right) = -\frac{\tau e^2}{r^2} \dot{\theta} + eA \cos(\theta - \omega t - \alpha) \quad , \quad (3)$$

where the radiation reaction has been attributed largely to the force from the Coulombic binding potential, and approximated as in Ref. [15], but now written in polar coordinates

above as:

$$\mathbf{F}_{\text{reac}} \approx \frac{2e^2}{3c^3} \frac{d}{dt} \left\{ \frac{-e^2 \mathbf{z}}{|\mathbf{z}|^3 m} \right\} = \hat{\mathbf{r}} \frac{2\tau e^2 \dot{r}}{r^3} - \hat{\boldsymbol{\theta}} \frac{\tau e^2 \dot{\theta}}{r^2} . \quad (4)$$

In order for a perfect circular orbit to be maintained, then we would need to impose that  $r = a$ ,  $\dot{r} = 0$ ,  $\ddot{r} = 0$ ,  $\theta = \omega t$ ,  $\dot{\theta} = \omega$ ,  $\ddot{\theta} = 0$ , then our NR approximation to  $\mathbf{F}_{\text{reac}}$  reduces to

$$\mathbf{F}_{\text{reac}} = -\hat{\boldsymbol{\theta}} \frac{\tau e^2 \omega}{a^2} = -\hat{\boldsymbol{\theta}} (\omega \tau) \frac{e^2}{a^2} = -\hat{\boldsymbol{\theta}} \left( \frac{\omega}{\omega_c} \right) e A_c . \quad (5)$$

Thus, the radiation reaction only occurs in the tangential direction for circular motion. It is clearly a very small force, since  $\tau \approx 6.3 \times 10^{-24}$  sec,  $\omega \approx 4.5 \times 10^{16}$  sec $^{-1}$  for  $a = 0.5 \text{ \AA}$ , so  $(\omega \tau) \approx 2.8 \times 10^{-7}$ , while  $e/a^2 \approx 1.9 \times 10^7$  statvolt is the magnitude of the Coulombic electrostatic field from the classical nucleus acting on the orbiting electron.

Equations (2) and (3) reduce to:

$$m\omega^2 a = \frac{e^2}{a^2} + eA \sin(\alpha) , \quad (6)$$

$$0 = -\left( \frac{\omega}{\omega_c} \right) e A_c + eA \cos(\alpha) . \quad (7)$$

Hence we have two equations and two unknowns, namely,  $\alpha$  and  $\omega$ . Solving for  $\omega$  yields the quadratic equation:

$$\omega^4 - 2\omega^2 \omega_c^2 \left[ 1 - \frac{(\tau \omega_c)^2}{2} \right] + \omega_c^4 \left( 1 - \frac{A^2}{A_c^2} (\omega_c \tau)^2 \right) = 0 , \quad (8)$$

which can readily be solved to obtain:

$$\omega^2 = \omega_c^2 \left\{ 1 - \frac{(\tau \omega_c)^2}{2} \pm (\tau \omega_c) \left[ \frac{A^2}{A_c^2} - 1 + \frac{(\tau \omega_c)^2}{4} \right]^{1/2} \right\} . \quad (9)$$

This solution is exact for our nonrelativistic case. To lowest order in  $(\tau \omega_c)$ , and where  $A/A_c$  is not just a very small fraction slightly larger than unity, then we can expand the above in terms of the small  $(\omega_c \tau)$  parameter to obtain

$$\omega^2 \approx \omega_c^2 \left\{ 1 \pm (\tau \omega_c) \left( \frac{A^2}{A_c^2} - 1 \right)^{1/2} \right\} , \quad (10)$$

where terms of order  $O[(\omega_c \tau)^2]$  have been dropped.

Turning to Eq. (7), we obtain

$$\alpha = \cos^{-1} \left( \frac{A_c \omega}{A \omega_c} \right) . \quad (11)$$

This result yields the exact value of  $\alpha$ . We of course assume  $A \geq A_c$ .

As for the  $\pm$  signs in Eqs. (9) and (10), one can show upon substituting back into Eqs. (7) and (6) that one needs to use the plus sign when  $0 \leq \alpha < \pi/2$ , and to use the minus sign when  $-\pi/2 < \alpha < 0$ . It should be noted that when  $\pi/2 \leq \alpha \leq \pi$ , or  $-\pi/2 \leq \alpha \leq -\pi$ , then the radiation reaction cannot be balanced by  $(-e) \mathbf{E}$  [see Eq. (7) or refer to Fig. 1] and infinite  $t_d$  is then not possible.

Thus, for each value of  $A$ , when  $A > A_c$ , there are two frequencies that we will call  $\omega_+$  and  $\omega_-$ , corresponding to the  $\pm$  signs in Eq. (9), and the two corresponding angles from Eq. (11) that we will call  $\alpha_+$  and  $\alpha_-$ , such that a perfect circular orbit can be maintained indefinitely for this idealistic situation. In Fig. 1, all vectors  $(-e) \mathbf{E}$  that can yield infinite stability lie in the top half semicircle ( $-\frac{\pi}{2} < \alpha < +\frac{\pi}{2}$ ). From Eq. (11),  $\alpha_+ = -\alpha_-$ . In Fig. 1,  $\alpha_+$  would be directed as shown, so  $\alpha_+ > 0$ , with  $(-e) \mathbf{E}$  tilted to the left of the velocity  $\mathbf{v}$ . The corresponding angular frequency of  $\omega_+$  would satisfy  $\omega_+ > \omega_c$ , where  $\omega_c$  is the angular frequency when  $\alpha = 0$  and  $A = A_c$ . Likewise,  $\alpha_-$  would be directed in Fig. 1 such that  $\alpha_- < 0$ , or,  $(-e) \mathbf{E}$  is tilted to the right of the velocity  $\mathbf{v}$ , with the corresponding angular frequency of  $\omega_-$  being such that  $\omega_- < \omega_c$ .

The differences between  $\omega_-$ ,  $\omega_c$ , and  $\omega_+$  are in general quite small, since the dimensionless quantity of  $(\omega_c \tau)$  is such a small number for most atomic radii of interest in Eqs. (9) and (10). For  $a = 0.5 \text{ \AA}$ ,  $(\omega_c \tau) = 2.8 \times 10^{-7}$ , so for this radius,  $\omega_+$ ,  $\omega_-$ , and  $\omega_c$  differ in the 7<sup>th</sup> decimal place for  $A = 10$  statvolt, the 5<sup>th</sup> decimal for  $A = 100$  statvolt, the 4<sup>th</sup> decimal for  $A = 1000$  statvolt, and the 3<sup>rd</sup> decimal for  $A = 80,000$  statvolt. Likewise, whether one used  $\omega_+$ ,  $\omega_c$ , or  $\omega_-$  in Eq. (11), will have a correspondingly small effect on  $\alpha_+$  and  $\alpha_-$ , with the most significant factor again being that  $\alpha_+ = -\alpha_-$ .

As can be shown, when  $A = A_c$ , then the + sign in Eq. (9) holds, and we obtain  $\omega = \omega_c$  and  $\alpha = 0$ , as expected. Moreover, since for reasonable values of  $A > A_c$  such that  $(\tau \omega_c)(A/A_c) \ll 1$ , then  $\omega_+ \approx \omega_- \approx \omega_c$ , so our exact NR result of Eq. (11) reduces to  $\alpha_{\pm} \approx \cos^{-1}(A_c/A)$ , with  $\alpha_+ = -\alpha_-$ .

What is interesting about these two solutions for a perfect circular orbit, is that the  $\omega_+$  solutions, with  $\pi/2 < \alpha_+ \leq 0$ , form what we will call “stable solutions”, meaning, that if one makes  $\alpha$  or  $\omega$  slightly less or greater than the prescribed values of  $\alpha_+$  and  $\omega_+$ , then one can still obtain a very long time before decay occurs; hence,  $t_d$ , although no longer infinite, will still be large. In contrast, the  $\omega_-$  solutions, with  $0 < \alpha_- < -\pi/2$ , form what we will

call “unstable solutions”, meaning, that if one makes  $\alpha$  or  $\omega$  slightly less or greater than the prescribed values of  $\alpha_-$  and  $\omega_-$ , then near immediate decay in the orbit begins. This result occurs even though the precise value of  $\alpha_-$  and  $\omega_-$  provide an orbit with an infinite value of  $t_d$ . The contrast seems fascinating, and will be discussed more in the next section involving detailed simulation results.

### III. SIMULATION STUDY OF $t_d$

In Ref. [15], simulation results were shown illustrating the very large range of  $t_d$  that can exist, simply by changing  $\alpha$ , while holding  $A$  fixed. Figure 2 illustrates the typical type of results found, this time for  $A = 300$  statvolt and  $\alpha = -\pi/4$ . We will define  $t_d$  precisely to be the point indicated in Fig. 2(b), which seems to be a key characteristic of the onset of orbital decay, namely, where the radial oscillation only rises to about the halfway point of previous oscillations, then starts to undergo a steady, oscillatory decline.

Using this definition of  $t_d$ , Fig. 3 shows our simulation results after carrying out calculations as in Fig. 2, for a range of values of  $\alpha$ , and for a range of values of  $A$ . These calculations were carried out for one frequency value of the applied CP plane wave, namely,  $\omega_c$ . More specifically, all trajectories were started in a circular orbit with  $a = 0.5 \text{ \AA}$ , with an applied CP plane wave with the indicated value of  $A$  and  $\alpha$  as in Fig. 3, and with an angular frequency  $\omega = (e^2/ma^3)^{1/2}$ . This is the proper frequency for a constant circular orbit (in the NR approximation) if either (1) no radiation reaction existed and no CP plane wave existed, or, (2) if radiation reaction existed, but  $A = A_c$  and  $\alpha = 0$ .

Four values of  $\alpha_+$ , from Eq. (11), corresponding to the values of  $A = 5.419, 6.0, 10,$  and  $1000$  statvolt, are labelled in this diagram. As can be seen, they fall at the center of the peaks of the  $t_d$  vs.  $\alpha$  curves. If the plane waves had the precise values of  $\omega = \omega_+$  from Eq. (9), then  $t_d$  would indeed be infinite (we have also confirmed this point via specific simulation testing). However, the simulations in Fig. 3 were carried out with the very slightly different value of  $\omega = \omega_c$  in the CP plane wave, so, the peaks of  $t_d$  vs.  $\alpha$  for these curves do not appear to be infinite, but, they are indeed very large and sharply peaked, and rather difficult to find exactly by pure simulation methods.

Moreover, in correspondence with the earlier comments made about the “unstable” peak at  $\omega_-$  and  $\alpha_-$ , no sign of the predicted infinite  $t_d$  peak shows up in Fig. 3, since  $\omega$  in the

plane wave expressions was not taken to be  $\omega_-$ , but rather the slightly different value of  $\omega_c$ . We should mention that our simulation testing of the “unstable peak” at  $\omega_-$  and  $\alpha_-$  does reveal its existence for each value of  $A$ , but, one needs to increase the precision of the numerical calculations to track the particle orbit out to larger time values; the higher the precision imposed, the farther out in time the simulation predicts before decay begins. It certainly appears that the  $t_d$  vs.  $\alpha$  curves do peak at  $\omega_-, \alpha_-$ , for each value of  $A$ , but, the shape of this peak appears like that of a near delta-function. Clearly, the behavior of  $t_d$  near the  $\omega_-, \alpha_-$  peaks is considerably different than the regions near the  $\omega_+, \alpha_+$  peaks.

Figure 4 helps to clarify the points made about the  $\omega_-, \alpha_-$  solutions. This figure contains our results for  $r$  vs.  $t$  based on numerically solving Eqs. (2) and (3) for  $a = 0.5 \text{ \AA}$  and  $A = 1000$  statvolt. As proven in Sec. II, the  $\omega_-, \alpha_-$  result should be exactly  $r = 0.5 \text{ \AA}$  for all  $t$ . However, as can be seen, the numerical predictions do not yield this result very easily. Here we followed the adaptive time-step Burlisch-Stoer algorithm, as described in Ref. [22], which we have found to be an extremely good algorithm to use when one plane wave is present. [All of our single plane wave numerical results reported here, and in Refs. [13], [14], and [15], used this algorithm.] The labels on the curves of “exp(-15)”, etc., indicate the relative precision we imposed on each step of the algorithm. As can be seen, even when huge increases in numerical precision were imposed, from exp(-15) to exp(-30), still, the simulation only yielded  $r \approx 0.5 \text{ \AA}$  up to about  $4 \times 10^{-14}$  sec, which is about 280 orbits; after that, the radius changed rapidly to about  $0.492 \text{ \AA}$ , and then a steady oscillatory radial decay began. In contrast, for the corresponding  $\alpha_+, \omega_+$  solution, even after  $5 \times 10^{-13}$  sec we found that the radius only fluctuated in value in the 7th decimal place when only a numerical precision of exp(-20) was imposed. Clearly, any “noise” present, such as from numerical imprecision, then the  $\alpha_-, \omega_-$  result will not be obtained, whereas the  $\alpha_+, \omega_+$  solution is far more easily approximated.

Some other interesting characteristics can be noted from Fig. 3. First, there are four peaks shown, corresponding to  $A = 5.419, 6.0, 10,$  and  $1000$  statvolt. For any fixed value of  $t_d$ , the widths of these peaks become increasingly broader, the larger the value of  $A$ . For example, for  $t_d = 5.0 \times 10^{-11}$  sec, the width of the  $A = A_c$  peak [i.e., the one indicated at 5.419 statvolt, from Eq. (1)] is zero, so this peak has the character of a delta function. In turn, the angular widths of the  $A = 5.419, 6.0, 10,$  and  $1000$  statvolt curves at  $t_d = 5.0 \times 10^{-11}$  sec in Fig. 3 become increasingly wider with increasing  $A$ , being approximately  $0, 0.07\pi,$

$0.16\pi$ , and  $0.30\pi$ , respectively.

Second, the  $t_d$  vs.  $\alpha$  curves for increasing values of  $A$  become increasingly more alike. For example, although not shown, we report here that the  $A = 80,000$  statvolt curve looks nearly identical to the eye to the  $A = 1000$  statvolt curve; only by zooming in somewhat would one detect a difference. Indeed, from Eqs. (11) and (9) one can prove that  $\alpha_+ \rightarrow +\pi/2$  as  $A \rightarrow \infty$ . Evidently, the shape of the  $t_d$  vs.  $\alpha$  curve, for  $\omega = \omega_c$ , as in Fig. 3, also goes to a limiting shape as  $A$  increases.

Third, it is interesting to note that for large values of  $A$  the places of  $t_d \approx 0$  are near  $\alpha = -\pi/2$ . For smaller values of  $A$ , such as for  $A = 6$  statvolt in Fig. 3, a region of values of  $\alpha$  exist where  $t_d > 0$ ; however, outside this region, one can see that  $t_d \approx 0$ , meaning that immediate decay sets in at the start of the simulation. In Fig. 3, the region of nonzero  $t_d$  values for  $A = 6$  statvolt extends roughly from  $\alpha = -0.14\pi$  to  $\alpha = 0.33\pi$ . It is interesting to note that the results from simulation of points where  $t_d$  curves go to zero on the left side of each peak, appear close in value to the position of the “unstable” infinite  $t_d$  peaks for  $\alpha_-$ ,  $\omega_-$  that can be calculated analytically.

For  $A \gg A_c$ , then as seen in Fig. 3, a very symmetrical pattern occurs about the horizontal axis in Fig. 1, with the longest decay time at  $\alpha \approx \pi/2$ , and the shortest decay time occurring at  $\alpha \approx -\pi/2$ . Figure 5(a) shows a way of organizing the effects of  $\alpha$  on  $t_d$  for this situation of  $A \gg A_c$ , where each pair of initial angles  $\alpha$ , such as would be given by  $A$  and  $A'$ ,  $B$  and  $B'$ , etc., in Fig. 5(a), have nearly the same value of  $t_d$  (for  $A = 1000$  statvolt), as well as nearly the same radial oscillatory amplitude. More specifically, for  $A \gg A_c$ , a curve of  $r$  vs.  $t$ , as in Fig. 2, has an initial oscillatory amplitude that is nearly zero for  $\alpha \approx \pi/2$ ; this is also the point at which  $t_d$  is largest. Similarly, for  $\alpha \approx -\pi/2$ , the initial oscillatory amplitude is at its largest value, with orbital decay setting in almost immediately.

Figures 5(b), 5(c), and 5(d) each compare the same “mirror” angles of  $\alpha = -\pi/4$  and  $\alpha = -3\pi/4$  in Fig. 5(a), and show how the  $r$  vs.  $t$  curves are nearly identical looking for  $A \gg A_c$  [i.e., Fig. 5(b) with  $A = 1000$  statvolt], but become progressively more different as  $A$  is decreased in Figs. 5(c) and 5(d), in correspondence with what we should expect from Fig. 3.

#### IV. ANALYTIC ANALYSIS OF $t_d$

We now turn to a more detailed analysis on the time to decay,  $t_d$ . In Ref. [15], we showed that by expressing  $r(t) = a + \delta(t)$  and the polar angle  $\theta(t) = \omega t + \phi(t)$ , where  $|\delta/a|$  is treated as being small compared to unity, and likewise for  $|\dot{\phi}/\omega|$ , then simplified and more easily analyzable differential equations in terms of  $\delta(t)$  and  $\phi(t)$  can be obtained than those of Eqs. (2) and (3). Several levels of approximation were discussed in Ref. [15], with what was called the ‘‘P2’’ level being the simplest approximation found that still provided a fairly good level of accuracy in most cases. In particular, case P2 predicted the key features of the oscillatory radial motion, namely, the increase in oscillatory amplitude with time, and the rapid change to orbital decay. The P2 set of equations were

$$\ddot{\phi} + \frac{3eA}{am} \left( 1 + \frac{2\dot{\phi}}{3\omega} \right) \cos(\phi - \alpha) - 3(\omega\tau)\omega^2 - 7(\omega\tau)\omega\dot{\phi} = 0 \quad , \quad (12)$$

combined with  $\frac{\delta(t)}{a} \approx -\frac{2}{3\omega}\dot{\phi}(t)$ , and the initial conditions of  $\phi = 0$ ,  $\dot{\phi} = 0$ , and  $\delta = 0$  at  $t = 0$ . These two equations and the initial conditions will enable us to make a simplified analysis of the transition point behavior at decay.

Figure 6(a) shows  $\phi(t)$  vs.  $t$  near the orbital transition region of decay when  $A = 1000$  statvolt and  $\alpha = -\pi/4$ . At each peak, of course  $\dot{\phi} = 0$ , and  $\ddot{\phi} < 0$ . As can roughly be seen, as the transition point to decay is approached, each peak becomes wider and wider, which means that the curvature becomes increasingly smaller, or  $|\ddot{\phi}|$  tends to zero. [This property of the peaks of the  $\phi$  vs.  $t$  curve gradually becoming wider and wider, the closer to the transition point, was first pointed out in Ref. [15]; see Fig. 4(c) in Ref. [15].] Thus,  $|\ddot{\phi}|$  decreases in magnitude from points A→B→C, with  $\ddot{\phi} < 0$ . At point D in Fig. 6(a), the transition point, the curve roughly goes through an inflexion point, with  $\dot{\phi} \approx 0$  and  $\ddot{\phi} \approx 0$ . This condition can be used as an approximate condition for calculating  $t_d$ .

From Eq. (12), with  $\ddot{\phi} \approx 0$  and  $\dot{\phi} \approx 0$ , then  $\cos(\phi - \alpha) \approx \frac{\omega^3\tau am}{eA}$ , or,

$$\phi(t = t_d) \equiv \phi_{\text{tran}} \approx \alpha + \cos^{-1} \left( \frac{\omega^3\tau am}{eA} \right) \quad . \quad (13)$$

For  $A = 1000$  statvolt,  $a = 0.5 \text{ \AA}$ , and  $\alpha = -\pi/4$ , then Eq. (13) predicts that  $\phi \approx 0.78$  at point D in Figs. 6(a), which agrees well with numerical calculations [see Fig. 6(b)].

Further insight can be gained if we define  $\Delta(t)$  to be the angle at time  $t$  between the velocity vector  $\mathbf{v}(t)$  of the electron and the force vector  $(-e)\mathbf{E}(t)$ . For the geometrical

situation chosen here (see Fig. 1), where the counterclockwise angular direction is taken to be positive, the particle starts at  $\hat{x}a$ , and  $\mathbf{v}(t=0)$  is along the  $\hat{y}$  direction, then  $\mathbf{v}(t)$  is at an angle  $\theta(t) + \frac{\pi}{2}$  with respect to  $\hat{x}$ , while  $(-e)\mathbf{E}$  at time  $t$  is at an angle with respect to  $\hat{x}$  of  $\alpha + \frac{\pi}{2} + \omega t$ . Hence:

$$\Delta(t) = \left[ \theta(t) + \frac{\pi}{2} \right] - \left( \alpha + \frac{\pi}{2} + \omega t \right) = \phi(t) - \alpha \quad . \quad (14)$$

The initial value of  $\Delta$  at  $t=0$  is  $-\alpha$ , since  $\phi=0$  at  $t=0$ . The angle  $\Delta(t)$  will initially vary between two points in Fig. 7(a). In the case of  $A \gg A_c$ , if  $\alpha$  is initially at point K in Fig. 5(a), then  $\Delta(t)$  will initially oscillate roughly (not quite, because the problem is not exactly symmetrical to either side of  $\alpha = +\pi/2$ ) between K' and K, with its center being approximately at the point of  $\phi=0$ ,  $\alpha = +\pi/2$ , or  $\Delta_{\text{mid}} = -\pi/2$ . However, the amplitude of the range of  $\Delta$  will gradually increase, as will, accordingly, the amplitude of  $\delta(t)$ , as observed in Fig. 2(a). Decay then sets in when  $\Delta(t)$  reaches the value of, from Eqs. (14) and (13)

$$\Delta(t=t_d) \equiv \Delta_{\text{tran}} = \cos^{-1} \left( \frac{\omega^3 \tau a m}{eA} \right) \quad . \quad (15)$$

Figure 7(a) illustrates the above, while Figs. 7(b) and 7(c) zoom in to show different aspects of the  $\Delta(t)$  vs.  $t$  curves.

As noted in Ref. [15], in the P2 approximation, the terms

$$\dot{\phi} \left[ \frac{2}{3\omega} \cos(\phi - \alpha) - 7\omega^2 \tau \right] \quad .$$

in Eq. (12) are the origin for the increasing amplitude of oscillation, the increase in periodicity [one can discern the latter feature in Fig. 7(c)], and the rapid transition to orbital decay. If it was possible to force these terms to equal zero, then case P2 will reduce to the approximate case O analyzed in Ref. [15], which predicts the initial oscillations very well, but never changes the oscillation shape and just continues on forever without orbital decay.

This insight offers another way to investigate situations in Fig. 3 where near infinite  $t_d$  occur. Forcing  $\dot{\phi} \left[ \frac{2}{3\omega} \cos(\phi - \alpha) - 7\omega^2 \tau \right]$  to be zero cannot be accomplished with one fixed value of  $\alpha$  if  $\phi$  is changing with time. However, it can be accomplished if  $\phi$  is made to be constant, by forcing  $\dot{\phi} = 0$ . The above term will then equal zero and the radial oscillations, via the P2 approximation of  $\frac{\delta(t)}{a} \approx -\frac{2}{3\omega} \dot{\phi}(t)$ , will then not change;  $r$  will then remain fixed at  $r = a$ .

Since in the situations examined here,  $\phi = 0$  at  $t = 0$ , then we can find the condition to make Eq. (12) result in  $\phi$  being constant for all time by substituting in zero for  $\phi$ ,  $\dot{\phi}$ , and  $\ddot{\phi}$ . Equation (12) then reduces to

$$\frac{3eA}{am} \cos(-\alpha) - 3(\omega\tau)\omega^2 = 0 \quad , \quad (16)$$

or, from Eqs. (1) and using  $\omega = \omega_c$ , since that was the basis of case P2 in Ref. [15], then

$$\alpha = \cos^{-1} \left( \frac{A_c}{A} \right) \quad . \quad (17)$$

This result agrees nicely with our earlier exact result of Eq. (11), since, as analyzed earlier from Eq. (10),  $\omega \approx \omega_c$ . Moreover, this analysis provides us another insight for points in Fig. 3 that lie near, but not right at  $\alpha = \alpha_+$ , namely, that when  $\dot{\phi}$  is small, which translates in the P2 approximation to  $\frac{\delta(t)}{a} \approx -\frac{2}{3\omega}\dot{\phi}(t)$  being small, or the radial oscillations  $|\delta/a| \ll 1$ , then we can expect a long time  $t_d$  before orbital decay sets in.

## V. CONCLUDING REMARKS

The present article began by noting that there exists a far larger range of conditions of infinite stability for a CP plane wave acting on a NR classical hydrogen atom, than the single case of  $\alpha = 0$  and  $A = A_c$  that was noted in Ref. [13]. Specifically, for each value of  $A > A_c$ , there are two values of  $\alpha$  such that a circular orbit will continue indefinitely in the highly idealized scenario described in the present article. If this classical scenario represented physical reality, then only one of these values, the  $\omega_+$ ,  $\alpha_+$  solution, would be readily observable, since any small deviation from the  $\omega_-$ ,  $\alpha_-$  solution appears to lead to near immediate orbital decay.

We should also clarify further the meaning of the “stable” solution of the  $\omega_+$ ,  $\alpha_+$  result, since any “noise” or other slight perturbation that enters the system, as of course would happen in a real physical situation, alters this otherwise perfectly aligned situation and appears to eventually lead to decay. Nevertheless, the size of  $t_d$  will still in general be quite large for small deviations from the idealized solution of  $\omega_+$ ,  $\alpha_+$ . Figure 3 helps to understand this point, since the simulations carried out in Fig. 3 did not use  $\omega_+$  as the frequency of the CP waves, but rather  $\omega_c$ , which is slightly different than  $\omega_+$ . We note that the widths and locations of the peaks of  $t_d$  vs.  $\alpha$  in Fig. 3 are quite interesting. As  $A$  approaches  $A_c$ , the width of the peak of  $t_d$  vs.  $\alpha$  becomes infinitesimally narrow.

Although we have not pursued the following idea in any sort of detail yet, it seems quite reasonable to us that most of the results analyzed here for circular orbits can be generalized to the more complicated situation of elliptical orbits, just as occurred in Refs. [13] and [14]. Reference [14] deduced the plane wave spectrum that would be required to overcome the radiation reaction effect to maintain an elliptical orbit, then turned to find the unexpected nonlinear behaviors that occur as the amplitudes of this plane wave spectrum were scaled. Likewise, we expect to find equally interesting results as phases are systematically altered. In turn, these relatively simple changes (e.g., scaling of amplitudes and systematic changes of phases) of electromagnetic radiation acting on the classical hydrogen model are but small subsets of the infinitely rich range of radiation conditions that could occur in a normal physical environment, in part from what an experimenter might ingeniously impose, as well as what naturally exists due to thermal and, more generally, nonequilibrium radiation conditions. Many recent experiments have already been carried out to examine such behaviors for actual Rydberg systems, such as in Refs. [8] and [23].

Finally, we wish to end this article by briefly mentioning other interesting nonlinear phenomena of this classical system. First, in Fig. 8(a), two CP plane waves were chosen to influence the orbital motion; their angular frequencies were selected to be slightly different, but close to the initial orbital angular frequency of the classical electron. As can be seen, “jump-like” motion was produced. It should be noted that approximately 10,000 orbits (the orbital period is about  $1.4 \times 10^{-16}$  sec for  $r = 0.5 \text{ \AA}$ ) occur for this simple scenario before the onset of orbital decay. During this time, four very clear and relatively rapid “jump-like” transitions occur. Adding more plane waves with similar changes in frequency can readily create an increase in jump-like behaviors, with larger jumps becoming more likely the larger the amplitude of the CP plane wave. Figure 9 illustrates this point of increasing the number of CP plane waves and its effect on quasi-stability. The quasi-stability region, up to the point of orbital decay, increased from about  $1.4 \times 10^{-12}$  sec to about  $5.0 \times 10^{-12}$  sec between Figs. 8(a) and 8(b), while the number of small “jumps” increased from four to about 25, and the number of orbits increased from approximately 10,000 to 36,000. Figure 8(b) is particularly interesting, in that it provides a conceptual way to see how stability can be roughly maintained, yet a region of radial dimensions can be sampled in a diffusion-like pattern.

Figure 9 illustrates “resonance-like” properties of plane waves acting on orbital motion.

Our earlier work in Refs. [13] and [14] analyzed related aspects of this phenomena for circular and elliptical orbits, respectively. One curve in Fig. 9(a) represents the case where an electron starts in a circular orbit of radius  $0.525 \text{ \AA}$ , with no plane waves acting ( $A = 0$ ), so that steady orbital decay occurs. The second curve in Fig. 9(a) represents a similar situation, but now where a CP plane wave is constantly acting, with  $A = 100$  statvolt,  $\alpha = 0$ , and an angular frequency corresponding to an electron in a circular orbit of  $0.5 \text{ \AA}$ . As can be seen, as the electron's orbit decays from  $0.525 \text{ \AA}$  to  $0.5 \text{ \AA}$ , the effect of the CP plane wave on the orbital motion becomes increasingly more pronounced, resulting in a jump-like behavior near  $r = 0.5 \text{ \AA}$ , followed by a continued fluctuating decay in orbit, but with fluctuations becoming increasingly smaller as the electron's radius steadily decreases below  $0.5 \text{ \AA}$ . Interestingly, the two radial curves for  $A = 0$  and  $A = 100$  statvolt are quite parallel to each other, aside from the fluctuating and jump-like behavior of the  $A = 100$  statvolt curve.

Figure 9(b) shows three curves pertaining to three different situations, each one where the electron has been “dropped” in a circular motion from an upper radius value, then allowed to decay to a lower radius while in the presence of a single CP plane wave, with  $A = 100$  statvolt and  $\alpha = 0$ ; in one case the angular frequency of the CP plane wave corresponds to a circular orbit of radius  $0.50 \text{ \AA}$  as in Fig. 9(a), while the other situations have the CP plane wave frequency corresponding to circular orbits of radius  $0.49 \text{ \AA}$  and  $0.48 \text{ \AA}$ , respectively. The  $y$ -axis of Fig. 9(b) represents the magnitude of the fluctuations of the radial motion [i.e., each peak minus each succeeding minimum in curves like the  $A = 100$  statvolt trajectory in Fig. 9(a)]. The intent of this figure is to attempt to characterize the “resonant-like” effect of plane waves acting on the electron's motion. As can be seen, the “response” in Fig. 9(b) is sharply peaked. We note that this response is a very nonlinear function, depending on several factors, including the radius and the amplitude of the CP plane wave. We intend to report on these effects in more detail in future work.

We have found such resonant, jump-like, and diffusion-like behaviors as seen in Figs. 8 and 9 to be fairly easy to produce, as well as a range of other interesting nonlinear phenomena, such as “catching” the electron, “kicking it” [24], [4], [23], etc. All of this work we expect to lead to greater understanding and insight into both practical technological possibilities as well as very basic and fundamental physical ideas. Clearly, there are surprising and subtle nonlinear effects that are difficult to anticipate, even for such simple cases as the

ones examined here involving simply a single CP plane wave acting on an electron in a near circular orbit.

Moreover, we have carried out numerous other simulation experiments attempting to go well beyond these simpler situations, by investigating the possibility of simulating the effect on the classical electron’s motion due to the hydrogen Coulombic binding force plus classical electromagnetic zero-point radiation, as well as due to other radiation fields of interest. In work to be reported elsewhere [21], we describe our simulation results to date for the classical hydrogen atom in the presence of classical electromagnetic ZP radiation. Most notably, this work has yielded a probability density distribution for the classical electron in close agreement with the quantum mechanical ground state of hydrogen from Schrödinger’s wave equation. Figure 10(a) shows a typical trajectory of a classical electron based on this simulation work, from which probability density distributions were calculated in Ref. [21]. The number of plane waves in the simulation of Fig. 10(a) was enormously larger than our earlier simpler examples in Fig. 8, namely, this simulation involves  $\approx 2.2 \times 10^6$  plane waves. The distribution of amplitudes and phases for these plane waves was chosen to represent a section of the classical electromagnetic ZP radiation spectrum. As can be seen in Fig. 10(a), the classical electron maintained a quasistability behavior, in that it’s orbit did not collapse into the nucleus nor ionize to infinity; however, it’s quasistability occurred in a stochastic manner, with it’s radius gradually increasing and decreasing due to the radiation’s effect on its motion.

Figure 10(b) shows more recent simulation results that differ from those of Ref. [21] in that a “window” algorithm approximation described in Ref. [21] is not imposed. The simulations in Fig. 10(b) only go out to about one-hundredth the time in Ref. [21], yet the computational time for Fig. 10(b) was about 50% larger than the already lengthy 55 CPU days reported in Ref. [21] on a Pentium 4, 1.8 GHz, processor (actual time 5 CPU days on 11 processors), due to the difference of the “no-window” versus “window” algorithm. In Fig. 10(b), an ensemble of nine classical electrons were started at  $0.53 \text{ \AA}$  and tracked over a time of  $2.87 \times 10^{-13} \text{ s}$ ,  $4.48 \times 10^{-13} \text{ s}$ ,  $8.20 \times 10^{-13} \text{ s}$  (about 2000, 3000, and 5000 revolutions, respectively) corresponding to each of the three curves in Fig. 10(b). As can be seen, the ensemble average is marching nicely toward the expected ground state distribution calculated from Schrödinger’s equation, which we expect to find once enough orbits have been tracked over to correspond with the longer runs in time in Ref. [21], where indeed this ground

state distribution was obtained. We expect to report in future work on the full results of this simulation experiment as well as considerably more extensive experiments presently in progress.

Undoubtedly, such results will come as a surprise to most physicists, as only classical electrodynamics is involved in these simulations. We note that the work discussed in the present article, as well as in Refs. [13], [14], [15], was critical in terms of developing the ideas and methods for carrying out such investigations to compare classical dynamical effects with quantum mechanical predictions. The work of the present article, which identifies the much wider range of stability conditions for the classical hydrogen atom under fairly simple applied radiation conditions, may well serve as the very beginnings for exploring statistical mechanical-like ideas for stability conditions that result in the ground state probability distribution found in Ref. [21]. These results cannot help but re-awaken the idea that the main basis of SED theory may in fact be correct [16], [17], [18]. Clearly, though, far more work needs to be done to examine all the other aspects of quantum mechanical phenomena for atomic systems, before this conclusion can be made; we are presently pursuing such investigations. Whatever the outcome, it should be quite clear that the range of classical physical behavior is extremely rich, as already revealed here by the very simple consideration of a classical charged particle in a near circular orbit about a classical nucleus, while acted upon by a single CP electromagnetic plane wave.

## ACKNOWLEDGEMENTS

We thank Prof. Timothy Boyer for reading the first draft of this article and for his encouragement and helpful suggestions.

- 
- [1] P. A. Braun. Discrete semiclassical methods in the theory of rydberg atoms in external fields. *Rev. Mod. Phys.*, 65(1):115–161, 1993.
  - [2] P. M. Koch and K. A. H. van Leeuwen. The importance of resonances in microwave “ionization” of excited hydrogen atoms. *Physics Reports*, 255:289–403, 1995.
  - [3] T. S. Monteiro, S. M. Owen, and D. S. Saraga. Manifestations of chaos in atoms, molecules and quantum wells. *Philos. Trans. R. Soc. Lond. Ser. A*, 357(1755):1359–1379, 1999.

- [4] S. Yoshida, C. O. Reinhold, P. Kristofel, and J. Burgdorfer. Exponential and nonexponential localization of the one-dimensional periodically kicked rydberg atom. *Phys. Rev. A*, 62:023408, 2000.
- [5] J. A. Griffiths and D. Farrelly. Ionization of rydberg atoms by circularly and elliptically polarized microwave fields. *Phys. Rev. A*, 45(5):R2678–R2681, 1992.
- [6] M. M. Sanders and R. V. Jensen. Classical theory of the chaotic ionization of highly excited hydrogen atoms. *Am. J. Phys.*, 64:21–31, 1996.
- [7] W. Schweizer, W. Jans, and T. Uzer. Optimal localization of wave packets on invariant structures. *Phys. Rev. A*, 58(2):1382–1388, 1998.
- [8] M. W. Noel, W. M. Griffith, and T. F. Gallagher. Classical subharmonic resonances in microwave ionization of lithium rydberg atoms. *Phys. Rev. A*, 62:063401, 2000.
- [9] C. Teitelboim, D. Villarroel, and Ch. G. van Weert. Classical electrodynamics of retarded fields and point particles. *Riv. del Nuovo Cimento*, 3(9):1–64, 1980.
- [10] P. A. M. Dirac. Classical theory of radiating electrons. *Proc. R. Soc. London Ser. A*, 167:148–169, 1938.
- [11] J. D. Jackson. *Classical Electrodynamics*. Wiley, New York, third edition, 1998.
- [12] F. Rohrlich. *Classical Charged Particles*. Addison–Wesley, Reading, MA, 1965.
- [13] D. C. Cole and Y. Zou. Simulation study of aspects of the classical hydrogen atom interacting with electromagnetic radiation: Circular orbits. *Journal of Scientific Computing*, 2003. , to be published Vol. 18, No. 3, June, 2003.
- [14] D. C. Cole and Y. Zou. Simulation study of aspects of the classical hydrogen atom interacting with electromagnetic radiation: Elliptical orbits. *Journal of Scientific Computing*, 2003. , Accepted for publication.
- [15] D. C. Cole and Y. Zou. Perturbation analysis and simulation study of the effects of phase on the classical hydrogen atom interacting with circularly polarized electromagnetic radiation. *Journal of Scientific Computing*, 2003. Submitted for publication. Preprint available at <http://www.bu.edu/simulation/publications/dcole/publications.html>.
- [16] T. H. Boyer. Random electrodynamics: The theory of classical electrodynamics with classical electromagnetic zero–point radiation. *Phys. Rev. D*, 11(4):790–808, 1975.
- [17] D. C. Cole. World Scientific, Singapore, 1993. pp. 501–532 in compendium book, “Essays on Formal Aspects of Electromagnetic Theory,” edited by A. Lakhtakia.

- [18] L. de la Peña and A. M. Cetto. *The Quantum Dice - An Introduction to Stochastic Electrodynamics*. Kluwer Acad. Publishers, Kluwer Dordrecht, 1996.
- [19] T. H. Boyer. Scaling symmetry and thermodynamic equilibrium for classical electromagnetic radiation. *Found. Phys.*, 19:1371–1383, 1989.
- [20] D. C. Cole. Classical electrodynamic systems interacting with classical electromagnetic random radiation. *Found. Phys.*, 20:225–240, 1990.
- [21] D. C. Cole and Y. Zou. Quantum mechanical ground state of hydrogen obtained from classical electrodynamics. 2003. Submitted for publication. Preprint available at <http://www.bu.edu/simulation/publications/dcole/publications.html>.
- [22] W. H. Press, S. A. Teukolsky, W. T. Vetterling, and B. P. Flannery. *Numerical Recipes in C: The Art of Scientific Computing*. Cambridge University Press, New York, second edition, 1992.
- [23] C. Wesdorp, F. Robicheaux, and L. D. Noordam. Displacing rydberg electrons: The mono-cycle nature of half-cycle pulses. *Phys. Rev. Lett.*, 87(8):083001, 2001.
- [24] S. Yoshida, C.O.Reinhold, and J. Burgdorfer. Quantum localization of the kicked rydberg atom. *Phys. Rev. Lett.*, 84(12):2602–2605, 2000.

## Figure Captions

Figure 1: Diagram at  $t = 0$  showing the initial orientation of the velocity vector  $\mathbf{v}$ , the electric force from the plane wave  $(-e) \mathbf{E}$ , the Coulombic binding force  $-e^2 \mathbf{r}/r^3$ , the negative of the centripetal acceleration times the mass,  $m\omega^2 \mathbf{r}$ , and the radiation reaction force [Eq. (5)], when the classical electron is beginning a circular orbit of radius  $a$ . By carefully selecting  $\alpha$ , for  $A > A_c$ , and by choosing the frequency  $\omega$  of the plane wave to match the orbital motion, then a perfect balance can be achieved.

Figure 2: (a)  $r$  vs.  $t$  for the classical electron in the scheme starting in the orbital condition of Fig. 1, with  $A = 300$  statvolt and  $\alpha = -\pi/4$ . The pattern shown here is fairly typical, namely, the amplitude of the radial oscillations gradually increase, the period also gradually increases [better seen in Fig. 2(b)], until finally orbital decay sets in. (b) A blown-up view is shown of the  $r$  vs.  $t$  curve in (a), near the point where orbital decay sets in.  $t_d$ , as indicated, is defined in this article as the point where the radial oscillation only rises to about the halfway point of previous oscillations, before beginning a steady, oscillatory decline. Up until the decay point, the period and amplitude of the oscillation gradually increases. The peaks change shape due to the nonlinear behavior, until finally the transition occurs. After the transition, the oscillations become smaller and smaller.

Figure 3: Plot of  $t_d$  vs.  $\alpha$ , for several conditions of  $A = 5.419, 6.0, 10,$  and  $1000$  statvolt. The points indicated along the curves were the ones actually calculated, using the method of Fig. 2(b). The dotted lines drawn were curve fits, put in to simply illustrate the trends better here. As analyzed in Sec. II, each of the curves have a near infinite peak for  $t_d$ . The peaks were drawn in here knowing their proper location from the analysis in Sec. II, but they were also verified by using these calculated peak positions in simulation runs to verify that  $t_d$  does appear to be infinite at these locations.

Figure 4: Plot of  $r$  vs.  $t$  with one CP plane wave present, attempting to numerically simulate one of the  $\alpha_-, \omega_-$  situations. The initial radius was  $0.5 \text{ \AA}$ . The conditions imposed on the CP plane wave were  $A = 1000$  statvolt, along with the values of  $\alpha_-$  and  $\omega_-$  as calculated from Eqs. (11) and (9). The adaptive time-step Burlisch-Stoer algorithm from Ref. [22] was used to compute  $r$  vs.  $t$ , for the different indicated relative precision conditions. As can be seen, even when a relative precision of  $\exp(-30)$  was imposed, the algorithm still only predicted that  $r \approx 0.5 \text{ \AA}$  up to about  $4 \times 10^{-14}$  sec, whereas the analytic solution

predicts that  $r = 0.5 \text{ \AA}$  for all time.

Figure 5: (a) A schematic figure is shown here to help better illustrate the effect of  $\alpha$  on both  $t_d$  as well as the amplitude of the spiralling motion, for the situation when  $A \gg A_c$ . Each pair of mirror points, such as A and A', B and B', have nearly the same value of  $t_d$  for  $A \gg A_c$ . Figures 5(b), 5(c), and 5(d) contain plots of  $r$  vs.  $t$ , for  $a = 0.5 \text{ \AA}$ . Each plot contains two  $r$  vs.  $t$  curves, one for  $\alpha = -\pi/4$ , and one for the ‘‘mirror case’’ of  $\alpha = -3\pi/4$ . (b)  $A = 1000$  statvolt; (c)  $A = 300$  statvolt; (d)  $A = 100$  statvolt. As can be seen, as  $A$  decreases, the behavior between the  $\alpha = -\pi/4$  and  $\alpha = -3\pi/4$  curves becomes increasingly different, in agreement with Fig. 3. For  $A = 100$  statvolt, the  $\alpha = -3\pi/4$  curve isn't even stable. Also apparent is the decrease in amplitude of the spiraling motion, and the decrease in  $t_d$  as  $A$  decreases.

Figure 6: Plots of  $\phi = \theta - \omega t$  are shown here for the case where  $A = 1000$  statvolt,  $a = 0.5 \text{ \AA}$ , and  $\alpha = -\pi/4$ . (a) The main curve to observe here is ‘‘Case E’’, where  $\phi(t)$  vs.  $t$  is shown for the ‘‘exact case’’, solving Eqs. (2) and (3). However, cases P1, P2, and O, which are different perturbation approximations discussed in Ref. [15], are also superimposed here to show how well they compare. (b) blown-up view of the transition point D in (a).  $\phi(t_d)$  is seen to agree reasonably well here with prediction.

Figure 7: Plots of  $\Delta(t) = [\phi(t) - \alpha]$  vs.  $t$ , for  $A = 1000$  statvolt, for several different values of  $\alpha$ . In (a), the ‘‘mirror’’ angles of  $\alpha = -3\pi/4, -\pi/4$ , as well as  $\alpha = 0, \pi$ , as well as  $\alpha = 3\pi/4, \pi/4$ , all have nearly identical values of  $t_d$ , which can be identified in 7(a) by the near vertical lines arising at the decay points in these curves [i.e.,  $\Delta(t)$  rapidly increases when orbital decay begins]. Note that  $\Delta(t_d) = \cos^{-1}\left(\frac{\omega^3 \tau a m}{eA}\right)$ , from Eq. (15), agrees well with prediction. Fig. 7(b) zooms into the early time region of 7(a) to show the differences between the  $\Delta(t)$  vs.  $t$  curves for  $\alpha = -\frac{3}{4}\pi$  and  $-\frac{1}{4}\pi$ , as well as  $\alpha = \pi$  and 0. Fig. 7(c) zooms in on the last region of the  $\Delta(t)$ .vs.  $t$  curve for  $\alpha = \frac{1}{4}\pi$ . Each of these  $\Delta(t)$  curves behave fairly similarly. The  $\Delta(t)$  vs.  $t$  curve for  $\alpha = \frac{1}{2}\pi$  can also be seen in 7(c), although its amplitude is still very small. As discussed in this article, if we were to repeat this examination for smaller values of  $A$ , one would see increasing differences in  $t_d$  for these ‘‘mirror’’ angles, since, as seen in Fig. 3, the  $t_d$  vs.  $\alpha$  curves become centered around different values of  $\alpha_+$  other than  $\pi/2$ , as  $A/A_c$  becomes smaller.

Figure 8: (a) Plot of  $r$  vs.  $t$  for the case where the initial radius is  $0.5 \text{ \AA}$ , and there are two CP plane waves present, both with  $\alpha = 0$ . One CP plane wave has  $A = 100$

statvolt, with an angular frequency corresponding to an orbital circular motion of radius  $0.5 \text{ \AA}$ , while the other has  $A = 500$  statvolt, with an angular frequency corresponding to an orbital circular motion of radius  $0.505 \text{ \AA}$ . The two horizontal lines indicate these radii. As can be seen, “jump” like motion occurs between the radii corresponding to these two angular frequencies. (b) Plot of  $r$  vs.  $t$ , as in (a), but now six CP plane waves are present, all with  $\alpha = 0$ . The circular orbital radii corresponding to their angular frequencies are indicated. These radii and the amplitudes of the plane waves are, respectively:  $0.485 \text{ \AA}$  and  $500$  statvolt;  $0.490 \text{ \AA}$  and  $500$  statvolt;  $0.495 \text{ \AA}$  and  $500$  statvolt;  $0.500 \text{ \AA}$  and  $100$  statvolt;  $0.505 \text{ \AA}$  and  $500$  statvolt;  $0.510 \text{ \AA}$  and  $500$  statvolt.

Figure 9: (a) Plot of  $r$  vs.  $t$  for two situations, both where the electron starts at  $r = 0.525 \text{ \AA}$ , but one where no CP plane wave is present ( $A = 0$ ), while the other case has a CP plane wave present with  $A = 100$  statvolt,  $\alpha = 0$ , and an angular frequency corresponding to an electron in a circular orbit of radius  $0.5 \text{ \AA}$ . (b) The maximum radius minus the minimum radius for each fluctuation in the  $r$  vs.  $t$  curve in Fig. 9(a), versus  $r$ , are plotted here for three situations. In each case the electron starts out in a circular orbit, with a CP plane wave acting, with  $A = 100$  statvolt and  $\alpha = 0$ ; the three curves are due to the presence of a single CP plane waves of angular frequency corresponding to a circular orbit of radius  $0.48 \text{ \AA}$ ,  $0.49 \text{ \AA}$ , and  $0.50 \text{ \AA}$ , respectively. As can be seen, these “response” curves are sharply peaked. Changing the amplitude of the applied CP plane wave changes the magnitude of this response, although the shape stays fairly similar for  $A$  not too large.

Figure 10: (a) Plot of  $r$  vs.  $t$  for a classical electron starting in a circular orbit of radius  $0.53 \text{ \AA}$ , with  $\approx 2.2 \times 10^6$  plane wave acting during the simulation. The amplitudes and phases were chosen at the beginning of the simulation and then held fixed throughout the remainder of the simulation. The values of these amplitudes and phases were chosen to represent one stochastic realization of a section of the classical electromagnetic ZP radiation spectrum. Ref. [21] discusses the specifics in more detail. (b) Nine classical electrons were tracked in time, each starting at  $0.53 \text{ \AA}$  in a circular orbit, but then subsequently not constrained. A different realization of the classical electromagnetic ZP radiation spectrum was assumed for each simulation, although all had  $771,692$  plane waves acting, ranging in angular frequency from  $5.0 \times 10^{17} \text{ s}^{-1}$  to  $4.6 \times 10^{11} \text{ s}^{-1}$ . The top three curves show the times up to which point the percentage of time was spent at each radius by the ensemble of nine electrons, as each evolved in trajectories like those in Fig. 10(a). The bottom curve was calculated from the

ground state of hydrogen via Schrödinger's equation:  $P(r) = 4\pi r^2 |\Psi(\mathbf{x})|^2 = \frac{4r^2}{a_B^3} \exp\left(-\frac{2r}{a_B}\right)$ , where  $a_B = \hbar^2/mc^2$ . Carrying these lengthy simulations out farther in time, we expect the histogram curves computed by simulation to converge closely to  $P(r) = \frac{4r^2}{a_B^3} \exp\left(-\frac{2r}{a_B}\right)$ , as they did in Ref. [21].

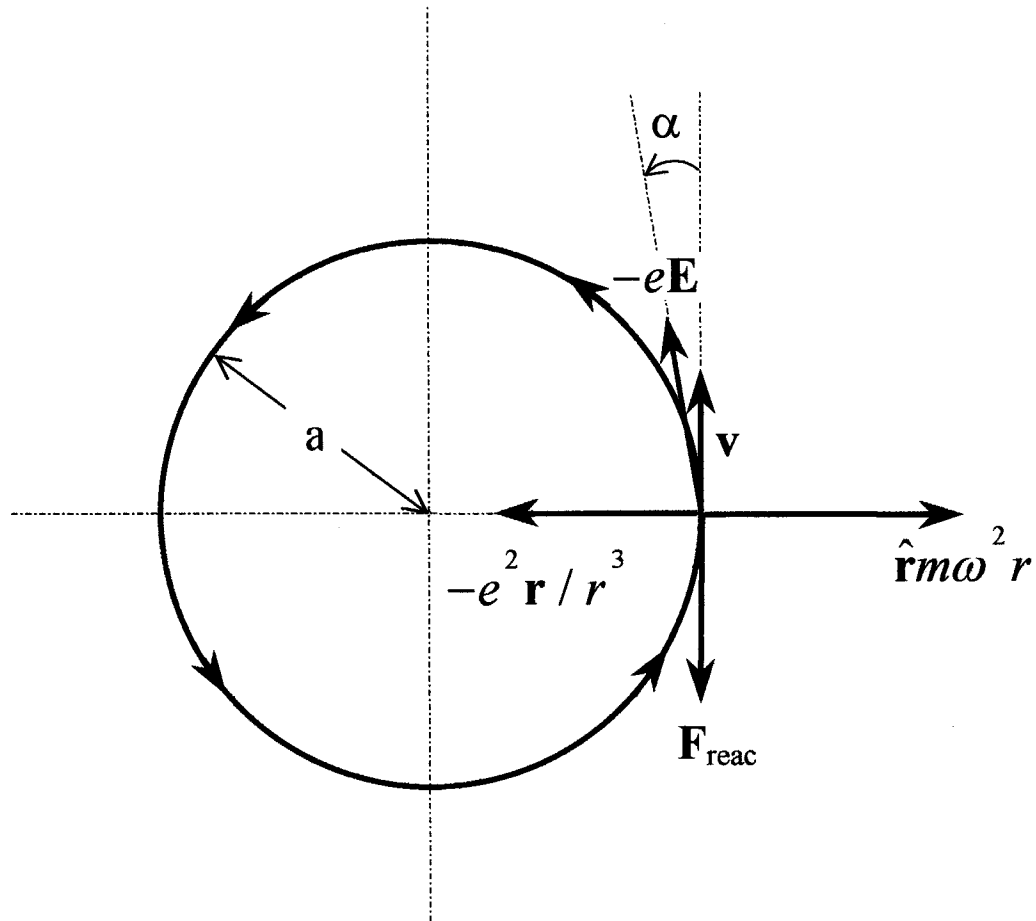


Fig. 1

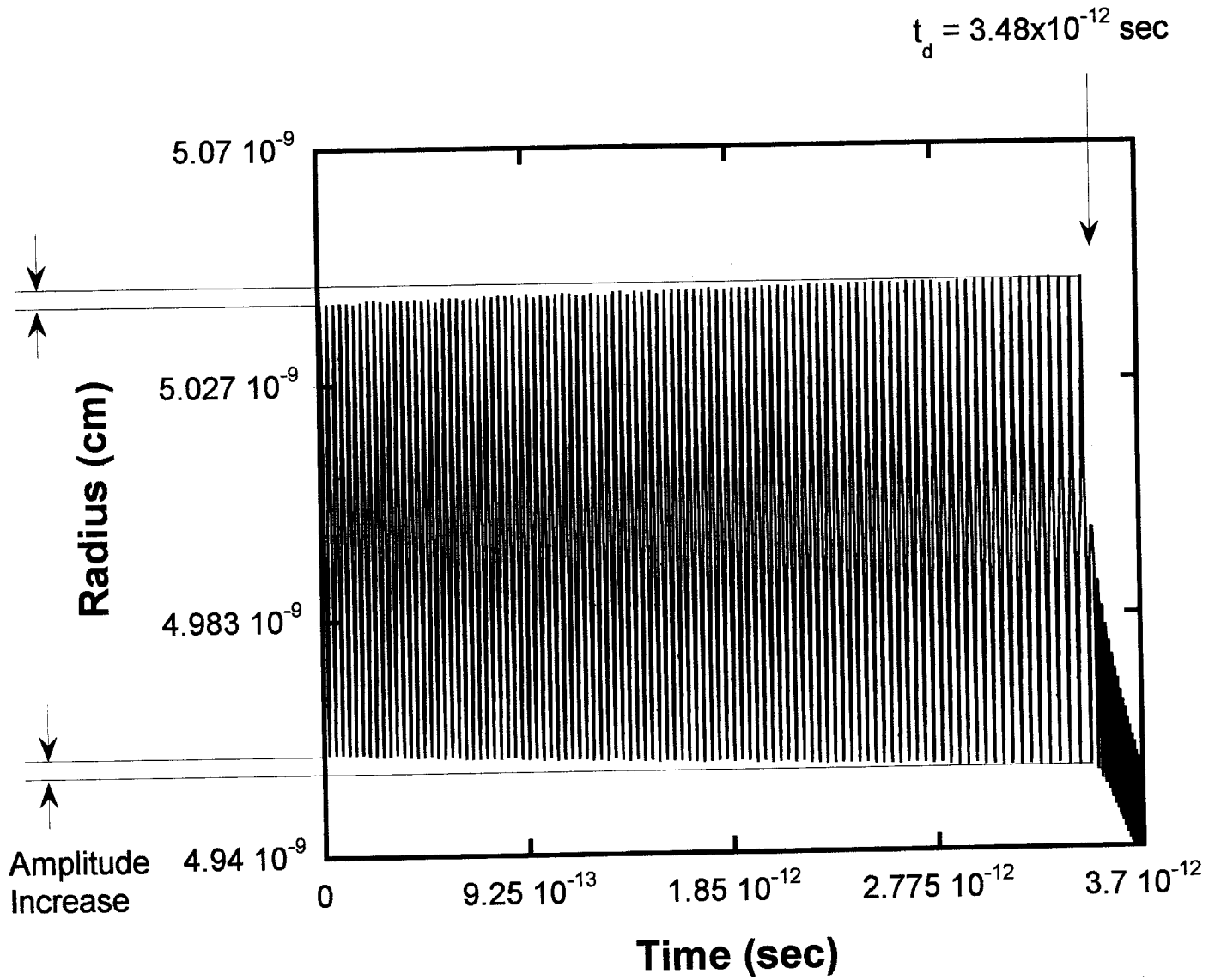


Fig. 2(a)

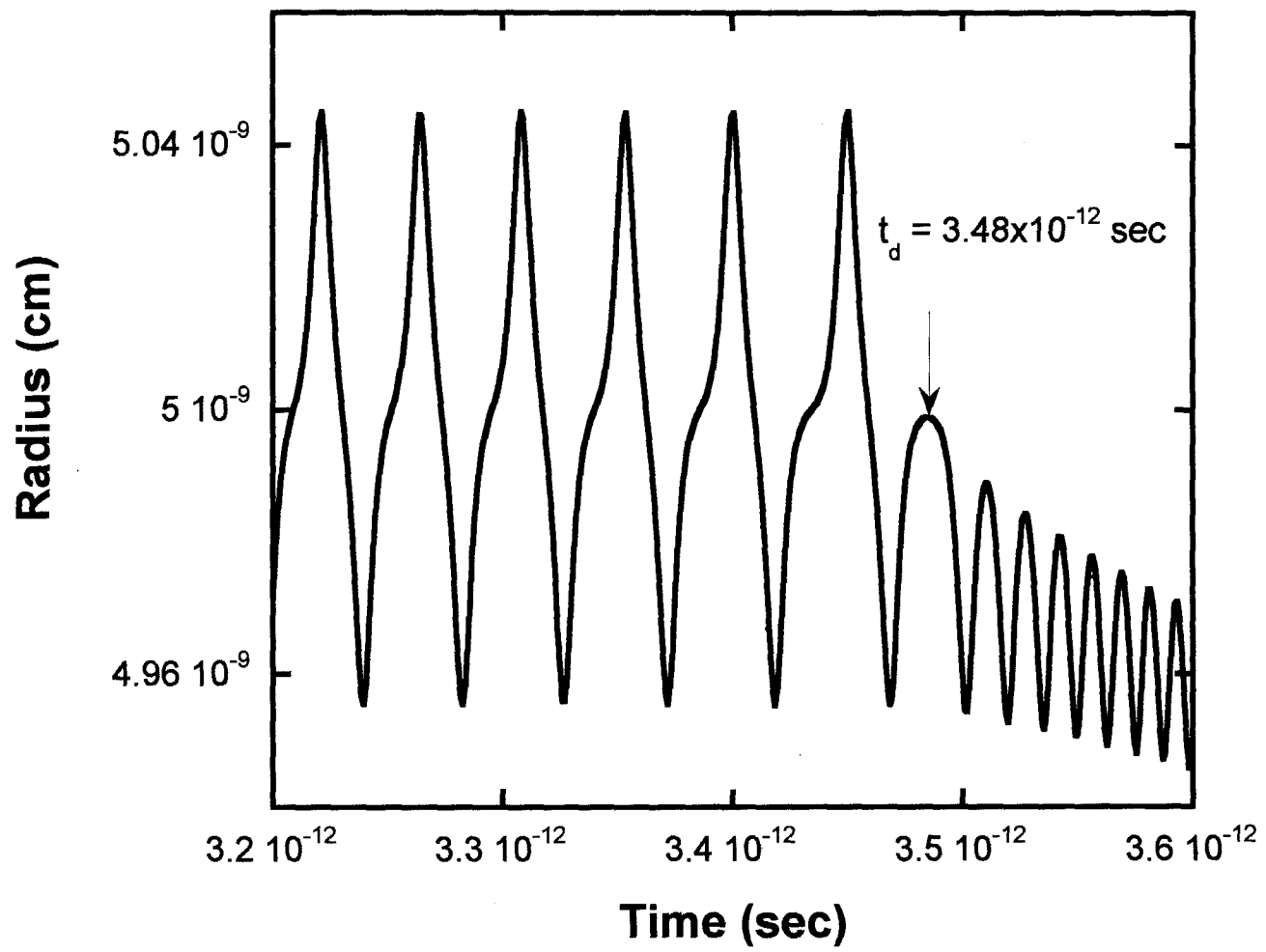


Fig. 2(b)

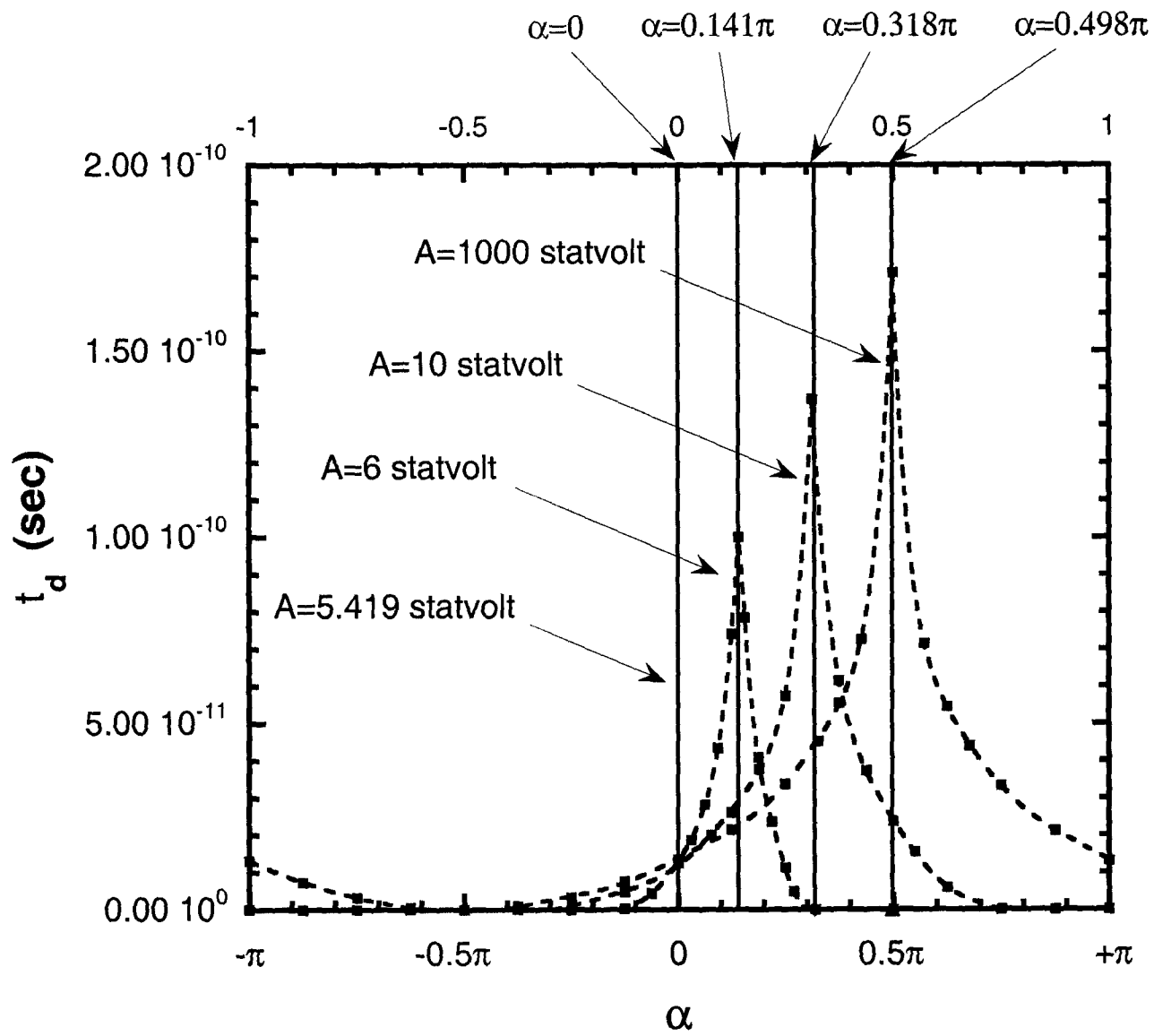


Fig. 3

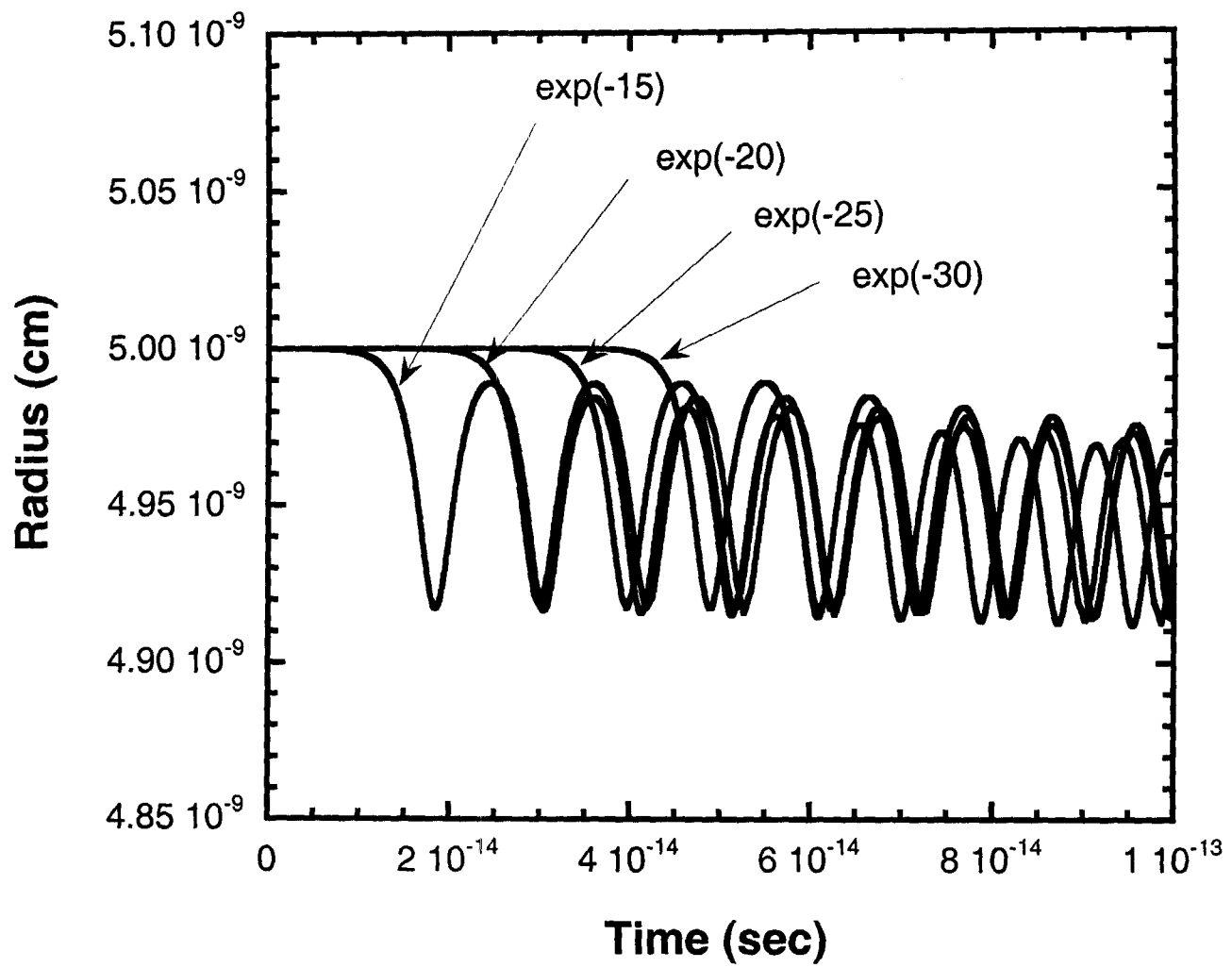


Fig. 4



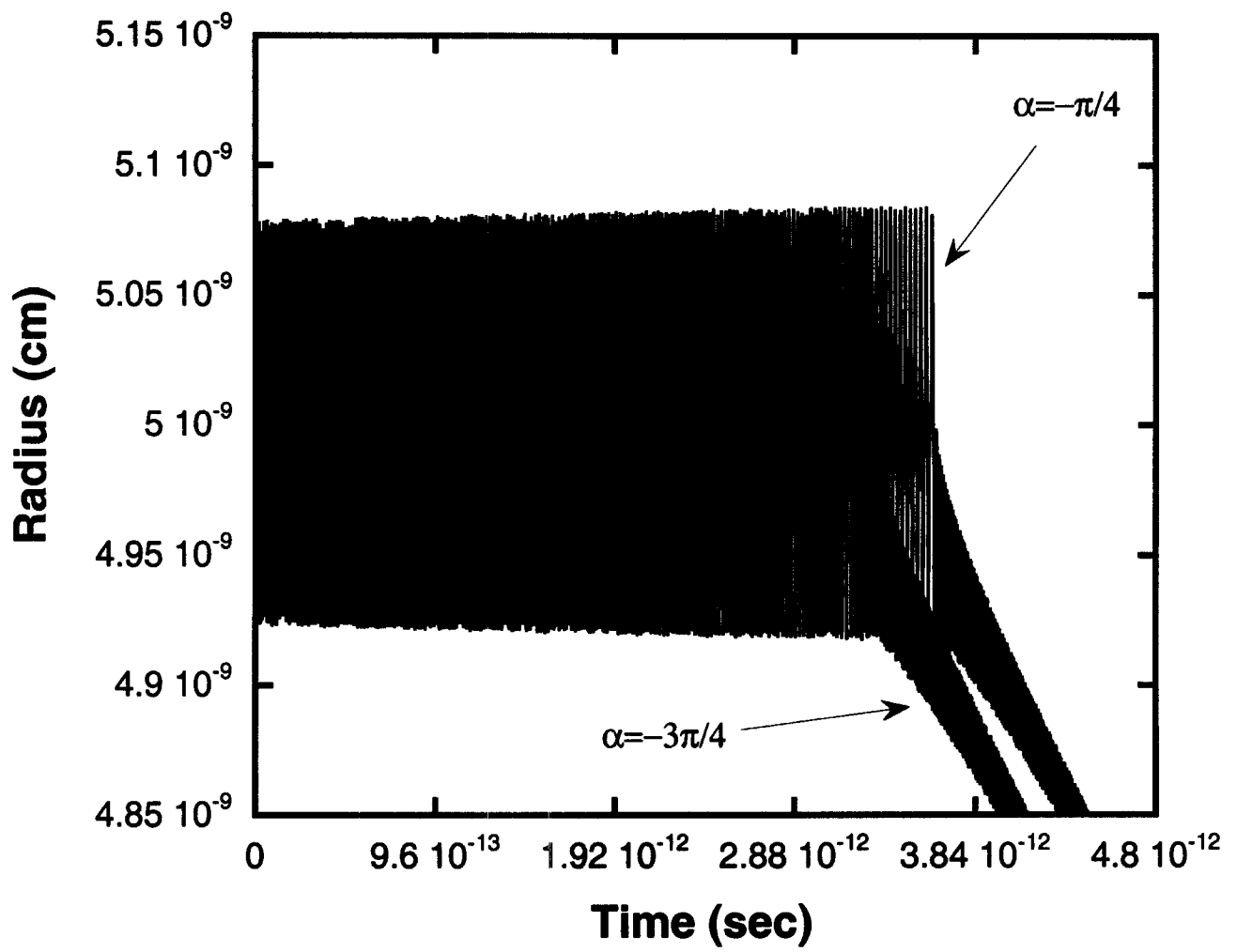


Fig. 5(b)

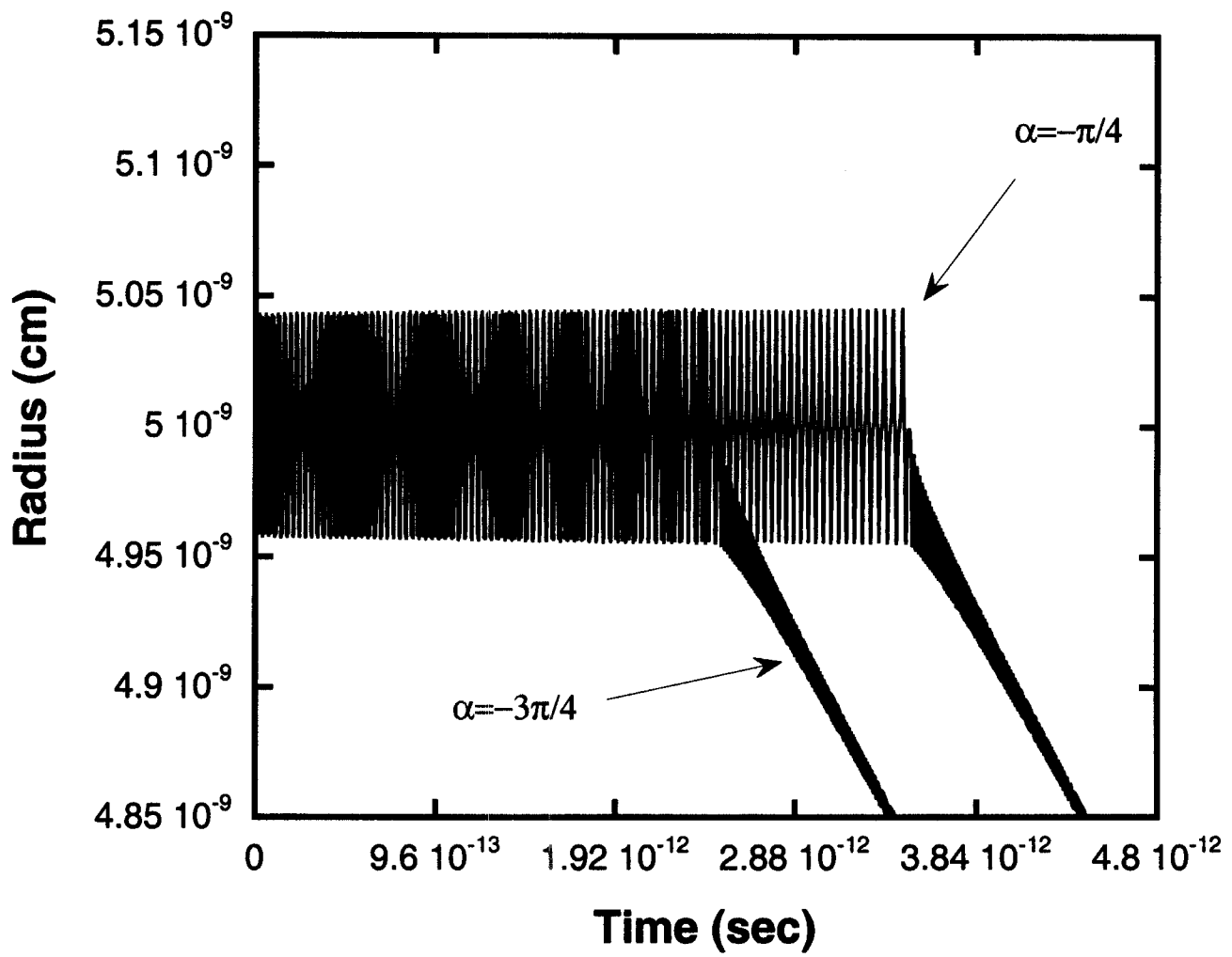


Fig. 5(c)

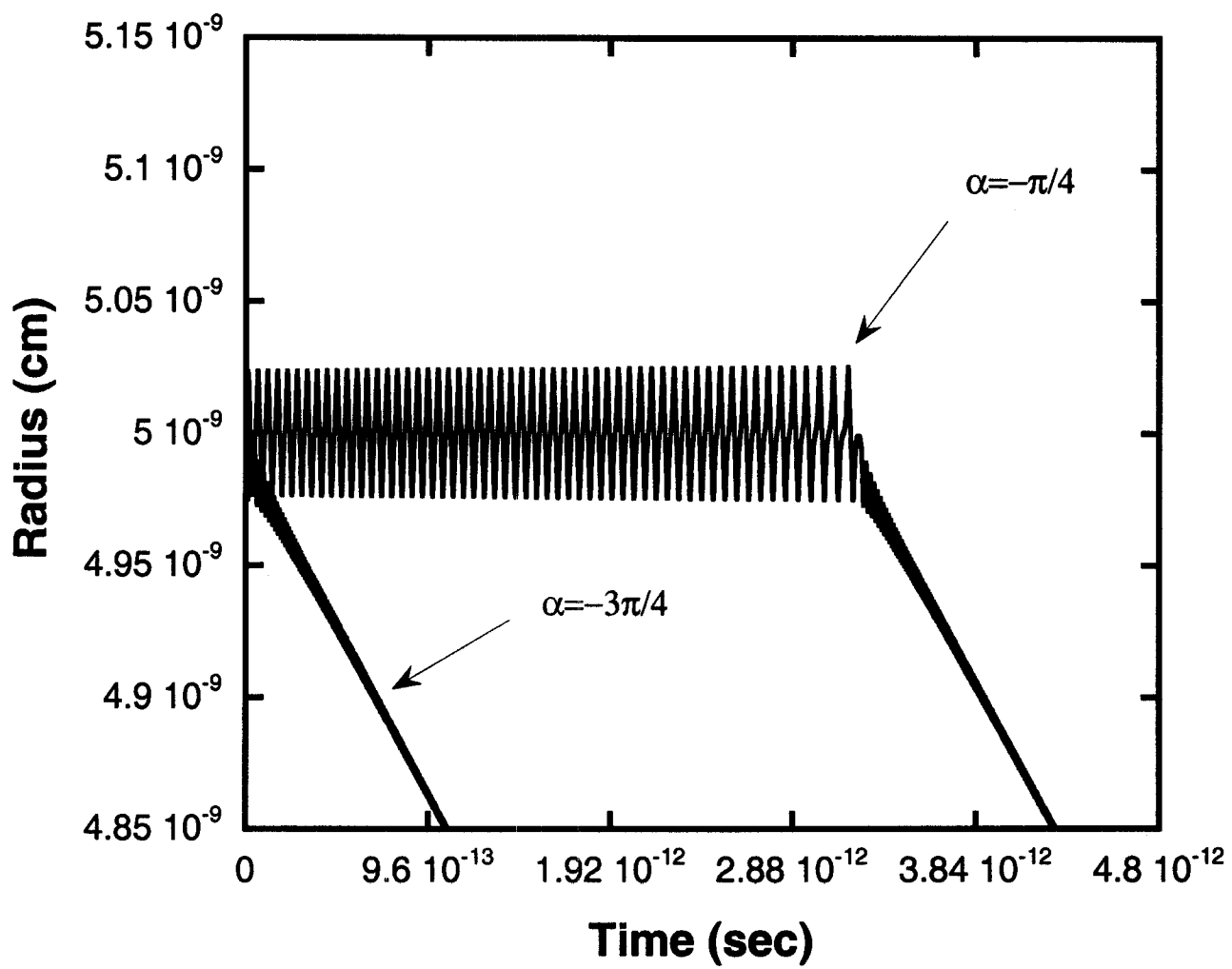


Fig. 5(d)

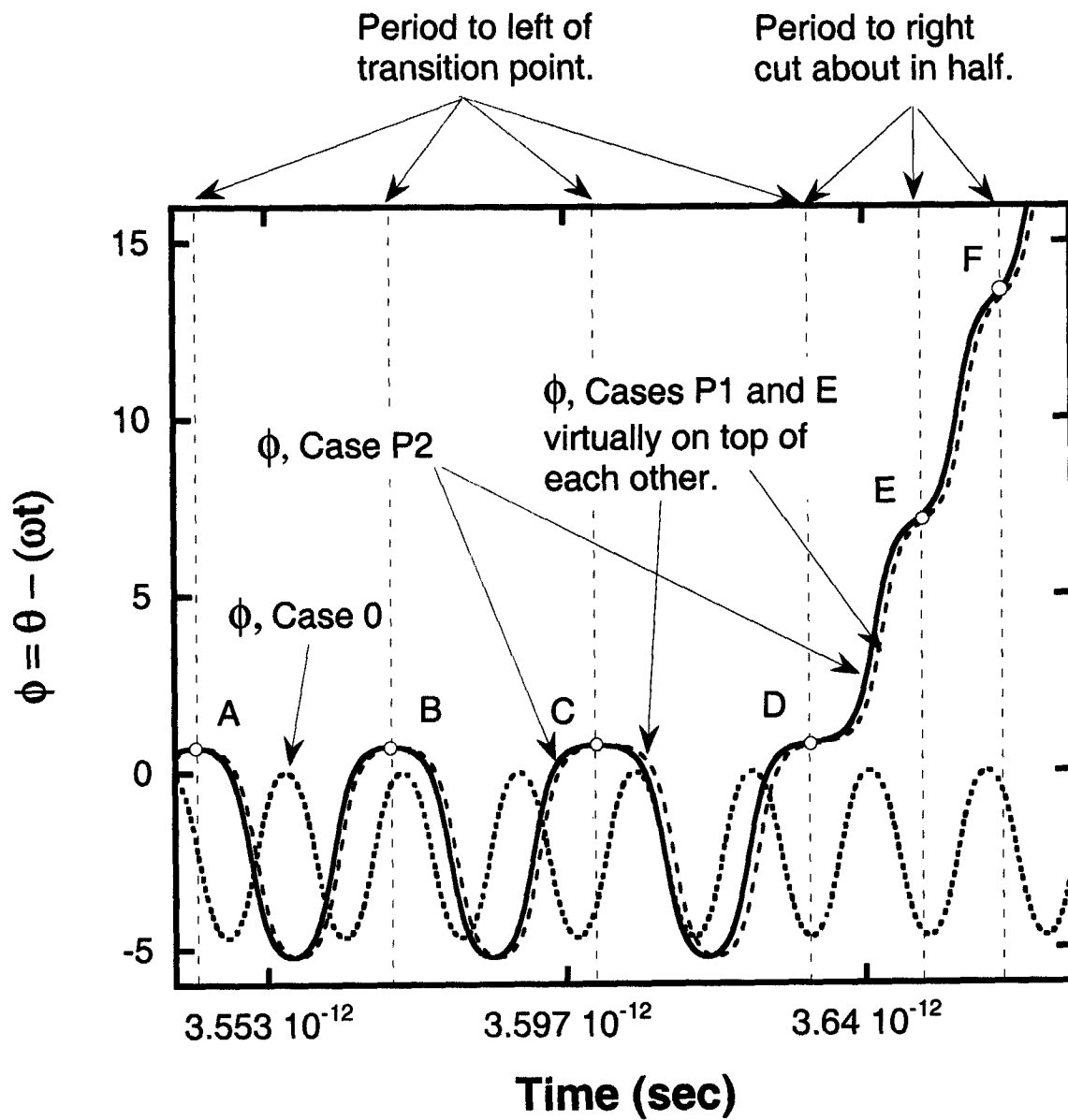


Fig. 6(a)

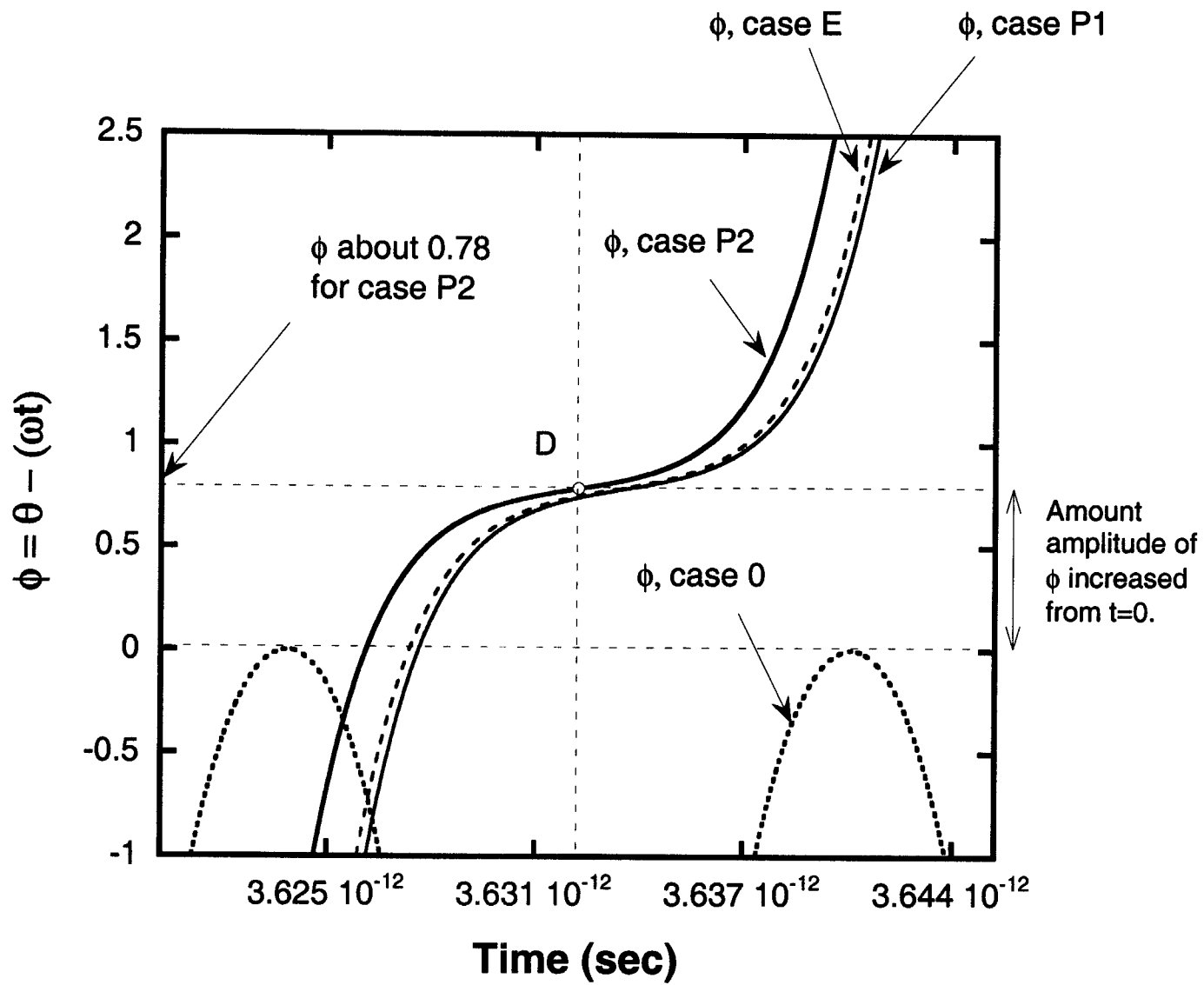


Fig. 6(b)

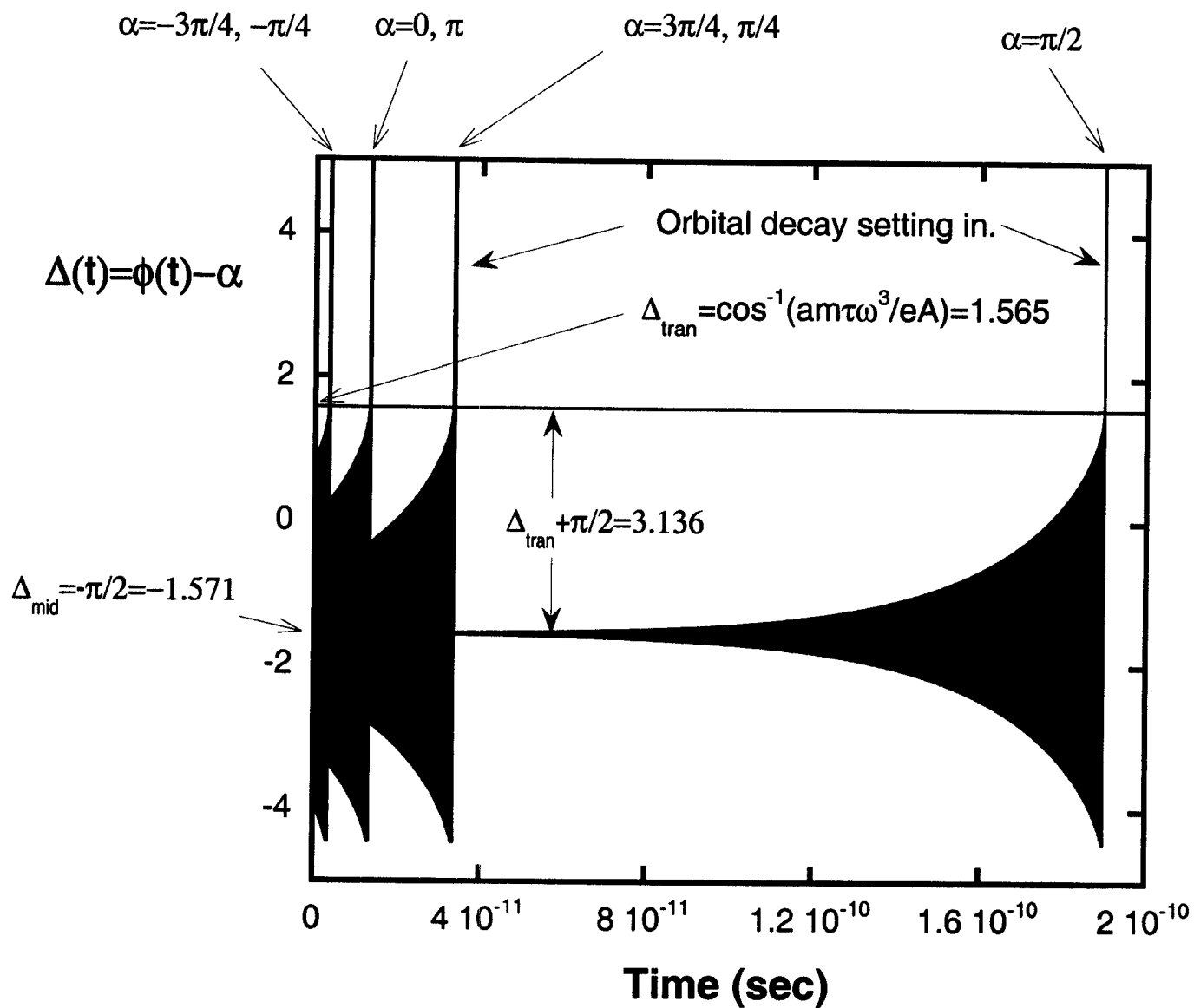


Fig. 7(a)

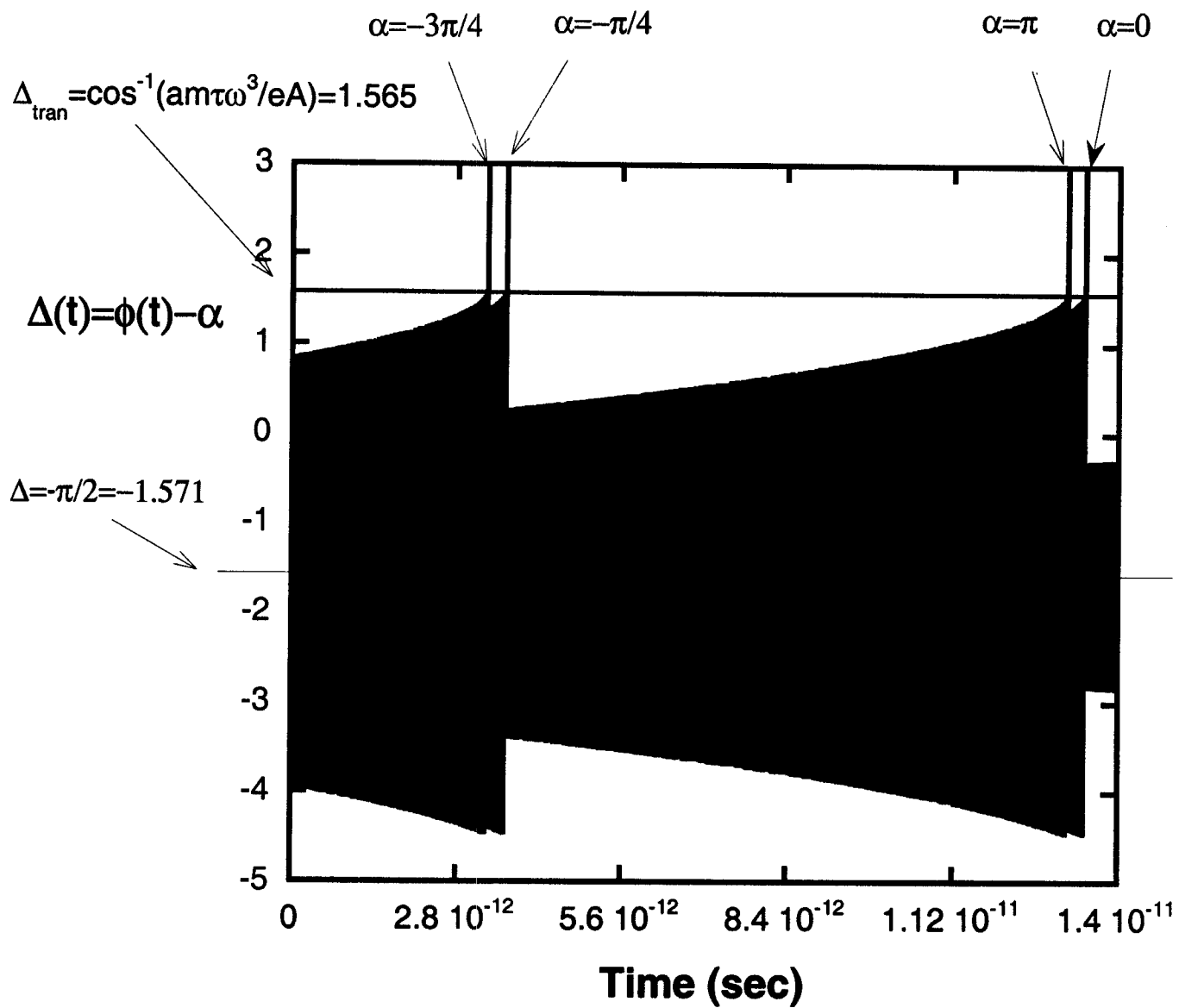


Fig. 7(b)

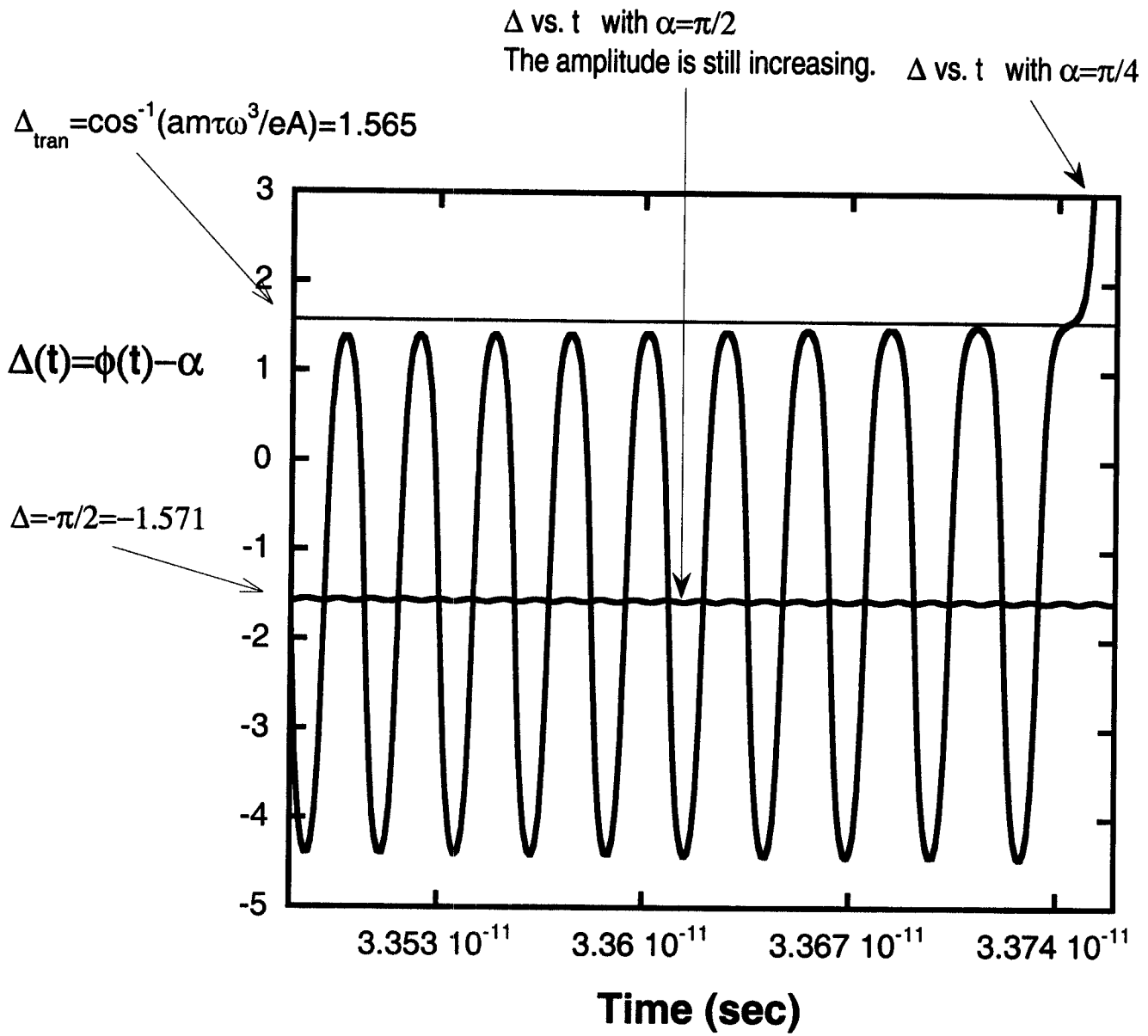


Fig. 7(c)

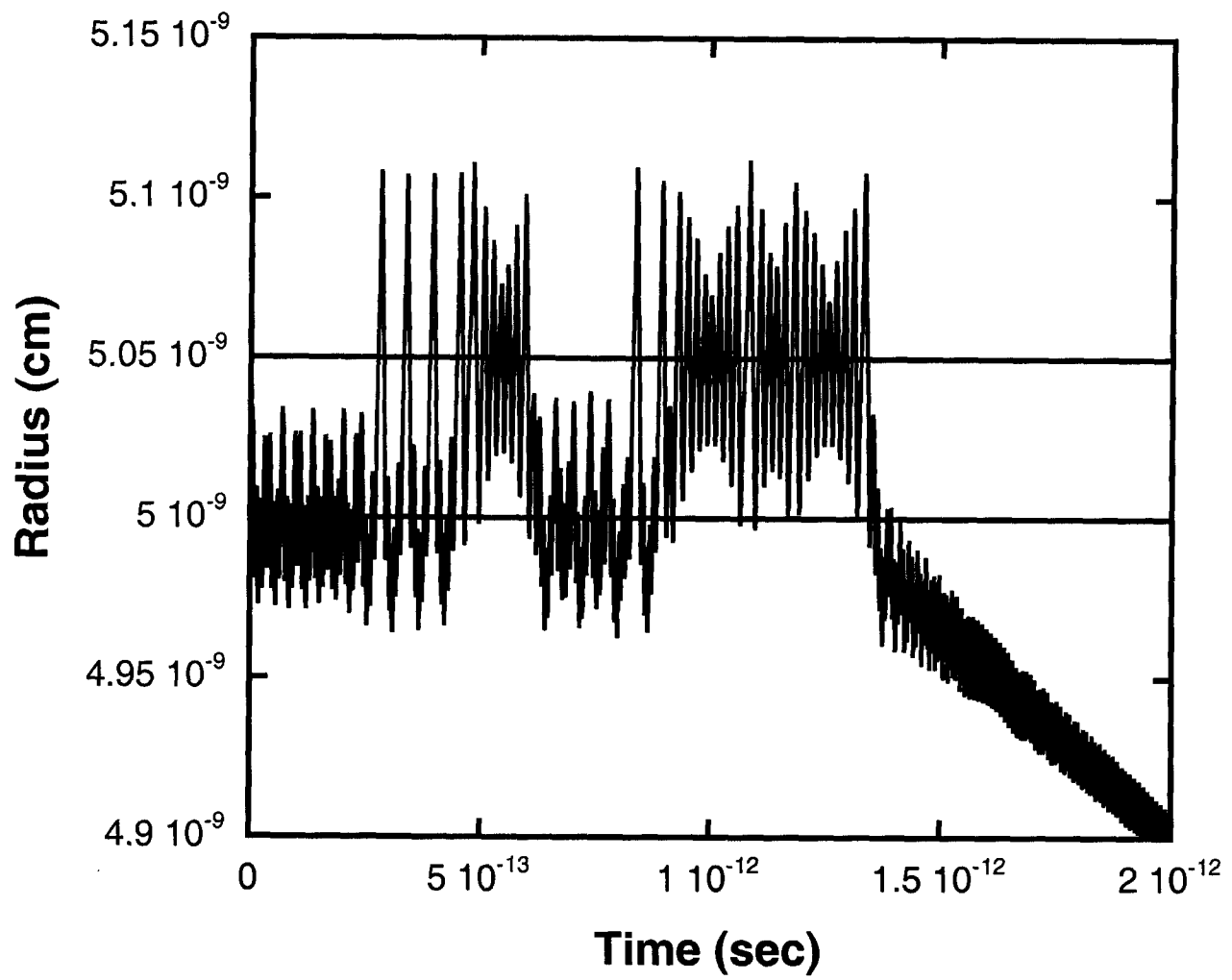


Fig. 8(a)

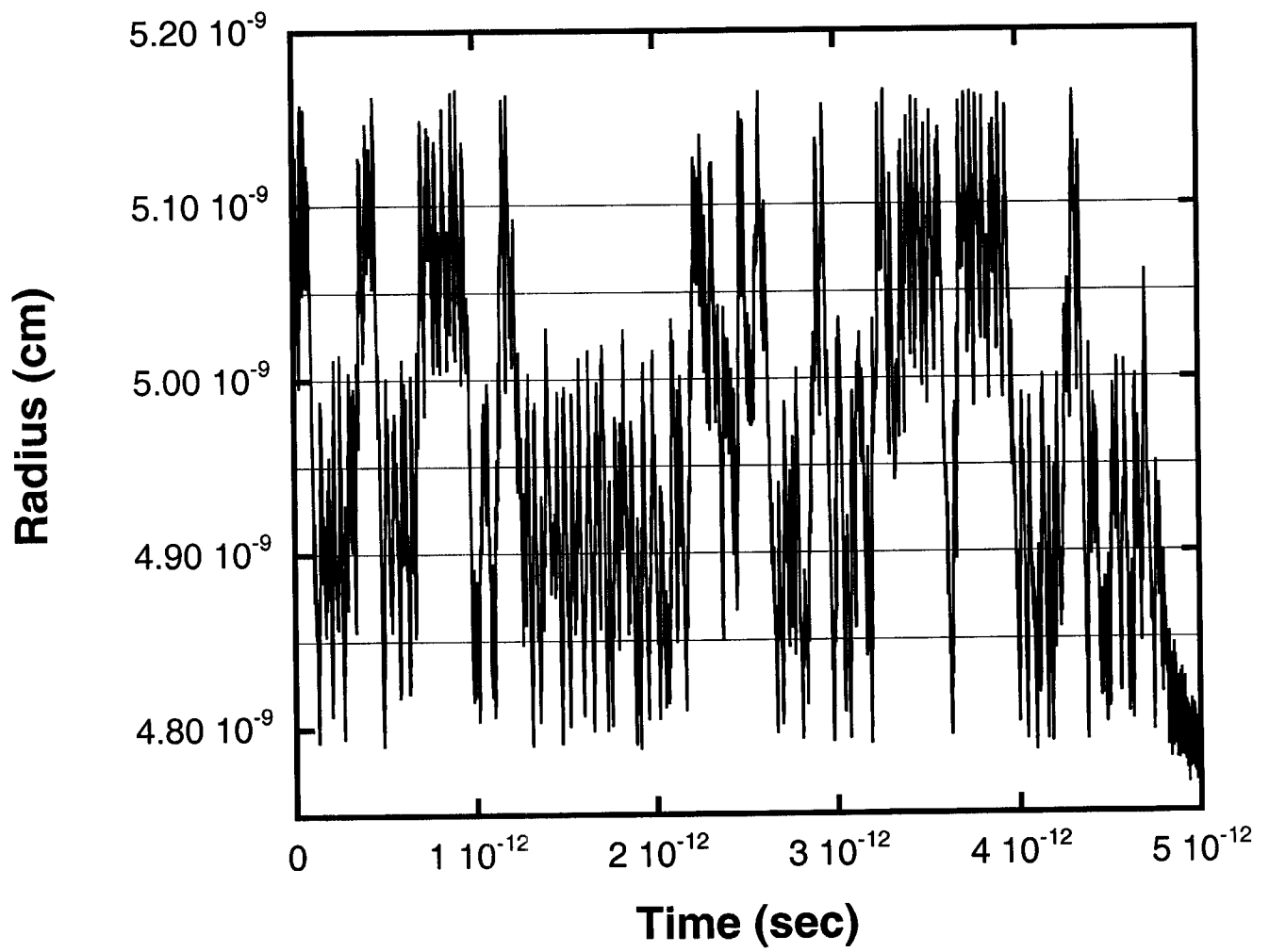


Fig. 8(b)

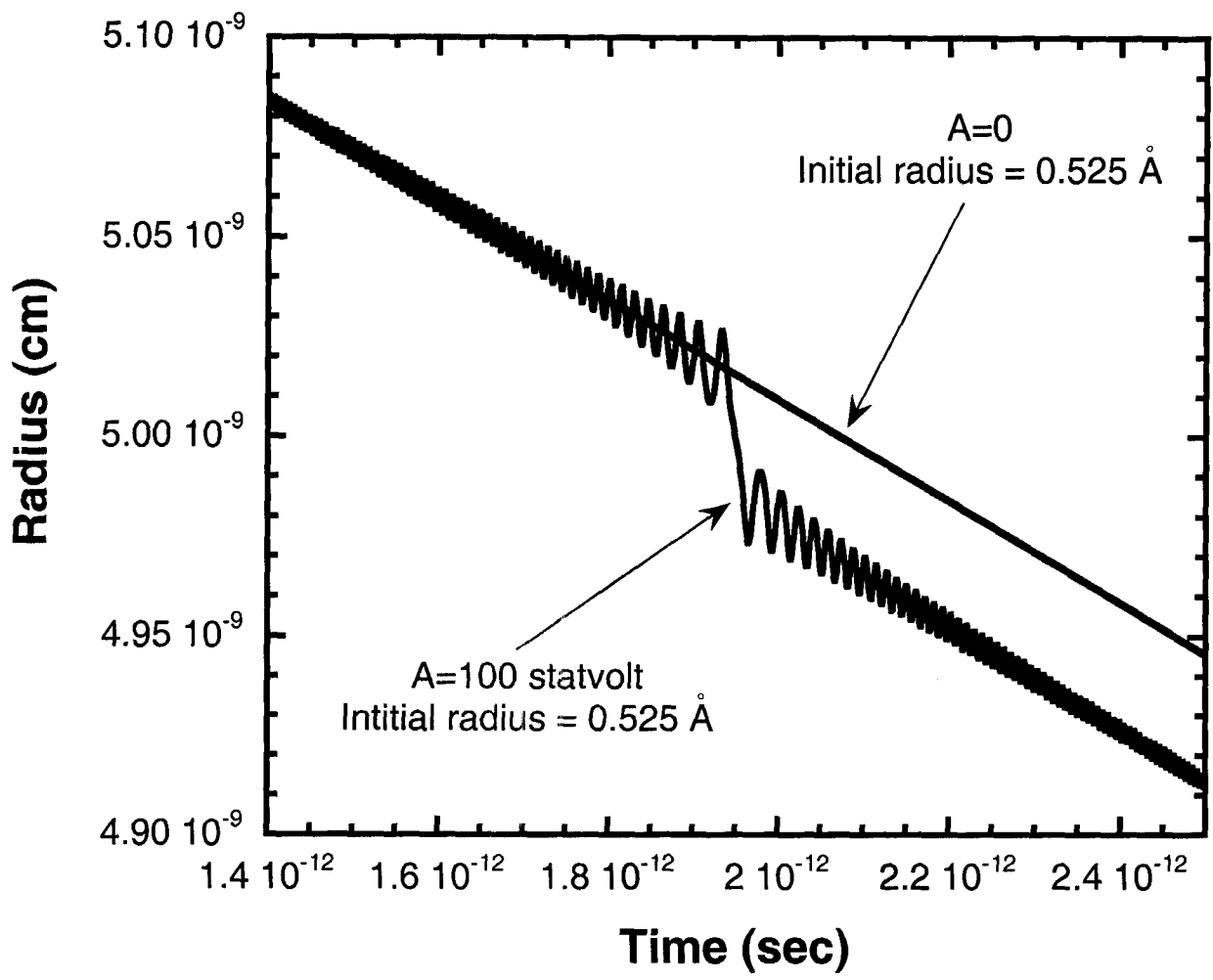


Fig. 9(a)

$[R_{\max} - R_{\min}]$  (cm)

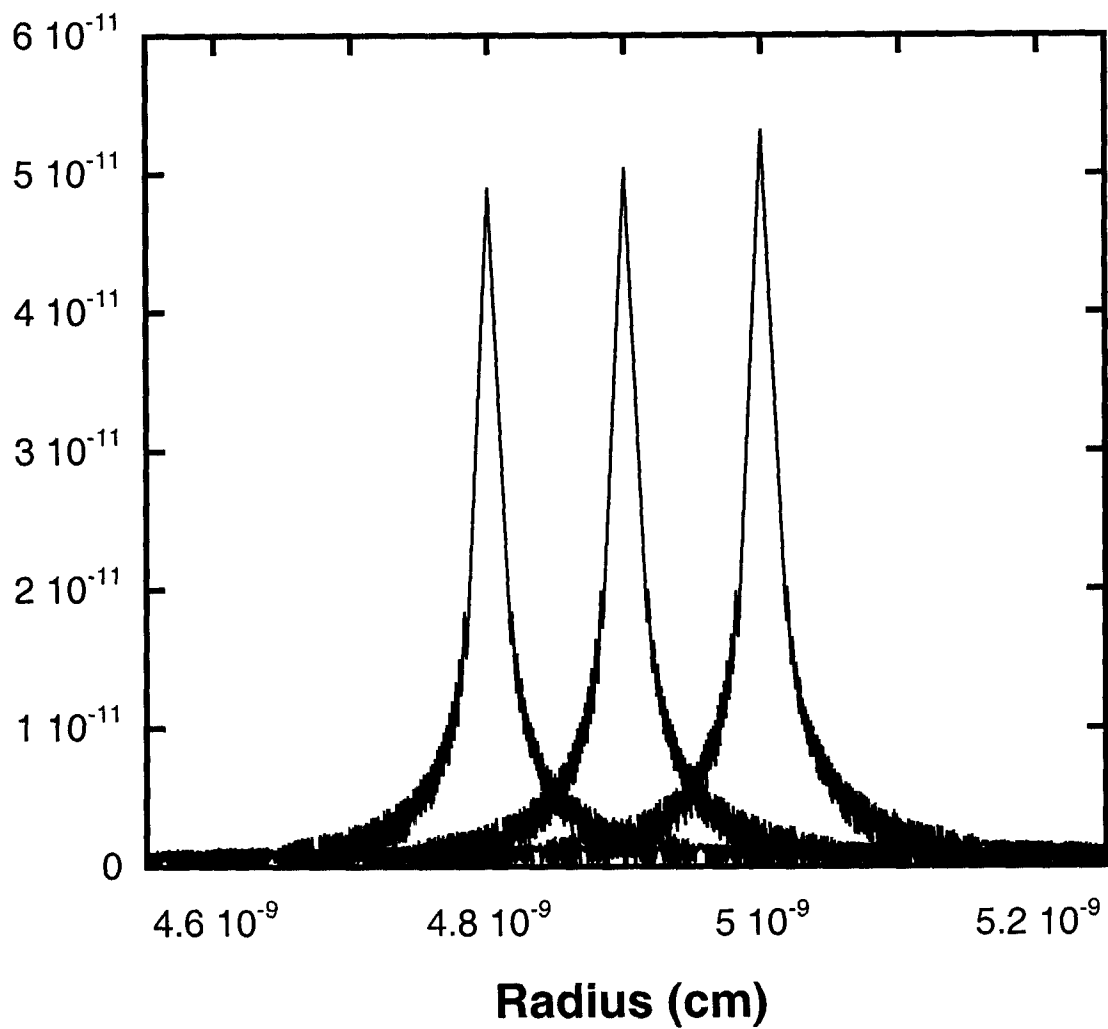


Fig. 9(b)

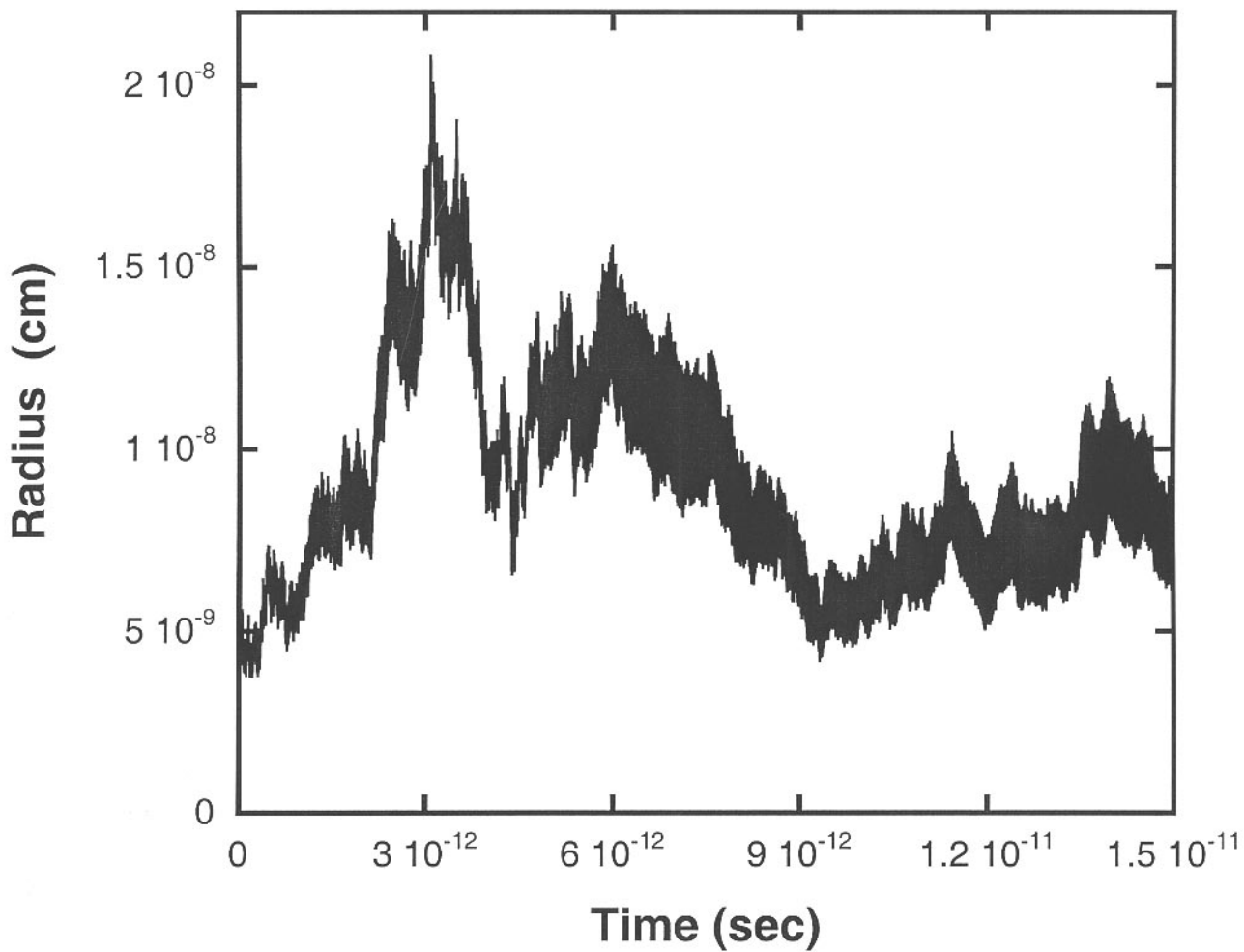


Fig. 10(a)

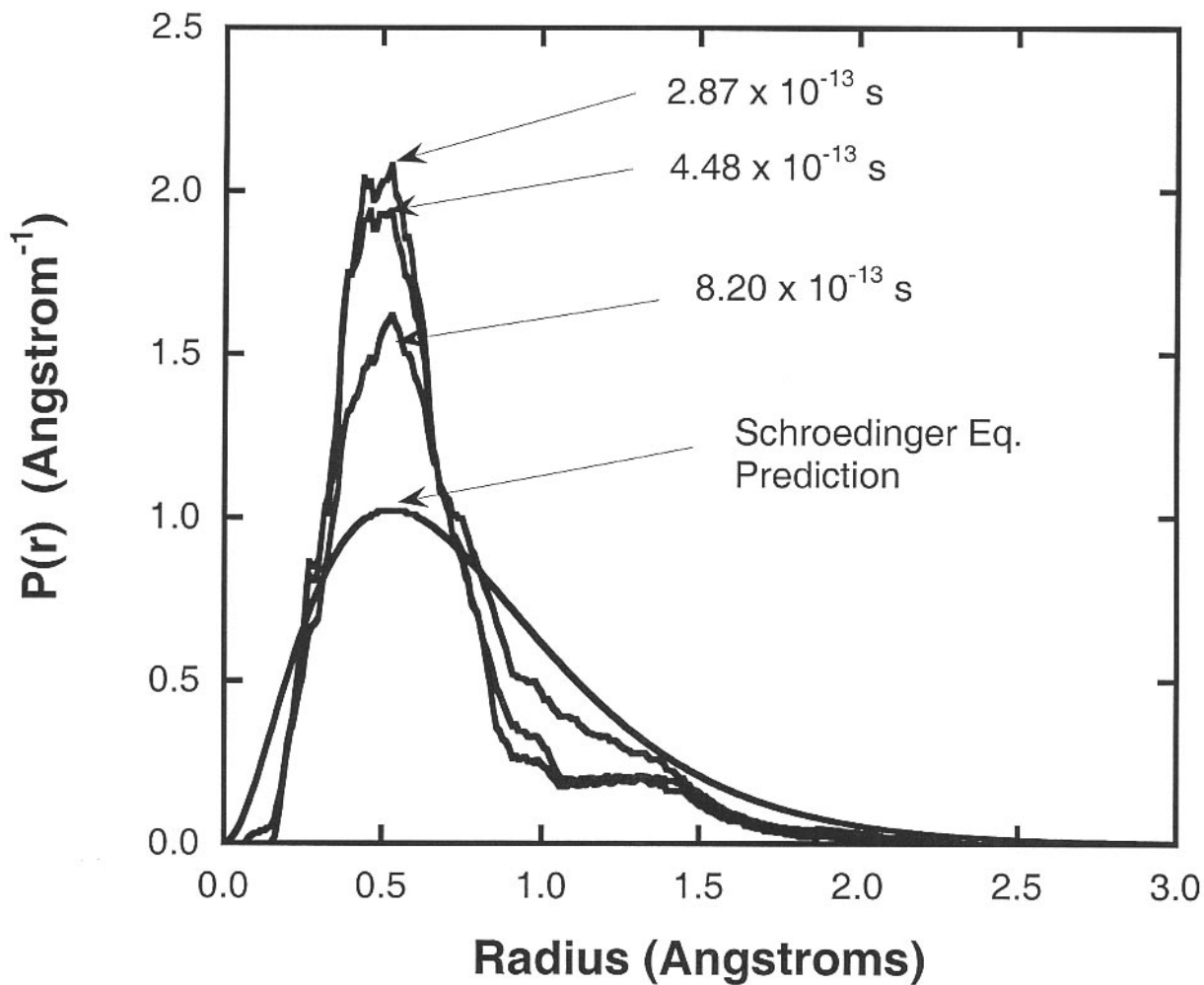


Fig. 10(b)